Properties of the strain-confined electron-hole liquid in Ge

J. P. Wolfe*
Physics Department, University of California, Berkeley, California 94720

R. S. Markiewicz,† S. M. Kelso, J. E. Furneaux, and C. D. Jeffries
Physics Department, University of California, Berkeley, California 94720
and Materials and Molecular Research Division, Lawrence Berkeley Laboratory, Berkeley, California 94720
(Received 9 February 1978)

A large volume of electron-hole liquid is formed by optically exciting a suitably stressed crystal of Ge. A contact stress produces a maximum shear region inside the crystal which acts as an attractive potential well for photoexcited carriers. Properties of the electron-hole liquid confined to this strain well are determined from spectral and spatial measurements of the recombination luminescence under wide variations in stress, temperature, and excitation level. Both electron-hole liquid and free-exciton phases are observed near 4 K, confirming the interpretation of a first-order liquid-gas phase transition and giving the exciton condensation energy $\phi \simeq 1$ meV. The liquid pair density at intermediate $\langle 111 \rangle$ stress is determined to be $(0.50 \pm 0.05) \times 10^{17}$ cm^{-3} from a luminescence line-shape analysis which takes into account the reduced electron band degeneracy and the strain-dependent hole mass. Magneto-oscillations in the luminescence intensity are observed which yield a similar density. A tenfold enhancement of the liquid lifetime is observed for stresses above 5 kgf/mm^2 and $1.8 \leq T \leq 4.2$ K, consistent with the reduced pair density and inhibited liquid evaporation in the strain well. Compression of the liquid at high excitation level is reflected in the line-shape, lifetime, and spatial imaging measurements. Time-resolved imaging of the liquid luminescence provides a striking contrast between the strain-confined liquid and the usual cloud of droplets in unstressed Ge.

I. INTRODUCTION

The electron-hole liquid (EHL) in semiconductors[1] represents a low-temperature phase transition of photoexcited electrons, holes, and free excitons (FE) into a uniform-density Fermi fluid. The properties of this unique liquid have been studied extensively over the past decade.[2] Most experiments to date have dealt with unstressed high-purity Ge, where a diffuse cloud of electron-hole droplets (EHD) (each ~1–10-μm size)[3] are formed. In a previous paper,[4] we showed that a large volume of EHL may be produced by carefully stressing a Ge sample, thereby confining the liquid to a maximum-stress region inside the crystal. This strain-confined liquid was termed a "γ drop," in contrast with the small "α drops" in unstrained Ge. A detailed analysis of the required macroscopic stress conditions was given. In this paper, we describe a number of luminescence experiments which determine the particular properties of the strain-confined EHL. We have observed luminescence from the gas of excitons in equilibrium with the liquid, thereby establishing the transition to the liquid phase. As expected, the properties of the strain-confined EHL, most notably the electron-hole (e-h) pair density n_γ, exciton condensation energy ϕ_γ, and e-h recombination lifetime τ_γ, are significantly different from those of EHD in unstressed Ge.

Evidence is presented here that for moderate excitation levels (corresponding to drop radii $\lesssim 150$ μm), the γ drop occupies a region of approximately uniform strain, so that the equilibrium properties may be studied. Larger drops are compressed by the strain well, resulting in an increased pair density and, consequently, a decreased pair-recombination lifetime. This compression affects most of our experimental results; a theoretical discussion of the EHL compressibility has been presented.[5]

While the properties of the EHL are expected to vary smoothly with uniform applied stress,[5] there are three distinct regimes under $\langle 111 \rangle$ compression. (i) The unstrained crystal, in which the electrons are equally distributed in four conduction-band valleys, and the holes are in two degenerate bands. In the notation of Ref. 4, we refer to this state as Ge(4:2); the numbers refer to the number of occupied conduction valleys and valence bands, respectively. Several calculations have been made of the properties of this state,[6-8] and the results are in good agreement with experiment.[2] (ii) Under moderate $\langle 111 \rangle$ compression ($3 \lesssim -\sigma \lesssim 10$ kgf/mm^2, where 1 kgf = 9.80665 N, and compressional stresses are taken to be negative) the conduction-band degeneracy is broken, and only a single valley is occupied. The two hole bands are partially split by the stress, but the splitting is less than the hole Fermi level. This state, Ge(1:2), is the principal object of the experimental study presented here. The results are in reasonable agree-

ment with theoretical calculations.[5,9] (iii) At higher stress ($-\sigma \gtrsim 10$ kgf/mm^2) one valence band is completely depopulated. This final state, GE(1:1), is theoretically expected[6,7,10] to have a considerably lower density than for the other states. In general, the stresses needed to observe this state are higher than those obtained in the present experiments.

In *nonuniformly* strained Ge, photoproduced EHD are attracted to regions of maximum shear strain. By applying a contact stress over a portion of the crystal surface it is possible to create one or more energy minima interior to the crystal.[4,11,12] This Hertzian contact stress[13] may be produced by applying a moderate force to the sample with a slightly rounded plastic plunger. Small EHD produced near the light excitation point are attracted to these potential wells and coalesce into masses of EHL. In Refs. 4 and 11 it was shown that the potential minima are located in regions of the crystal where the local strain tensor is approximately equivalent to a ⟨111⟩ uniaxial strain. This is because the electronic deformation potential in Ge is largest for a uniaxial strain along the ⟨111⟩ axis. If the contact force is applied along a direction other than ⟨111⟩, potential minima occur along ⟨111⟩ axes radiating out from the point of contact. Thus 1, 2, or 4 drops are produced when the contact force is applied along ⟨111⟩, ⟨110⟩, or ⟨100⟩ directions, respectively. These multiple drops are found to have similar properties irrespective of the direction in which the contact force is applied, consistent with the idea that in each case the potential minima correspond to a local ⟨111⟩ uniaxial strain.

The formation of large volumes of strain-confined liquid is a phenomenon quite distinct from the usual EHD formation in unstressed Ge. If an unstressed sample of Ge is illuminated by a laser beam focused to a point, the EHD produced by the light will form a cloud[14,15] of small droplets which increases in size as the laser intensity is increased. Experiments reported here—infrared imaging, kinetic studies, and spectroscopy—show that a cloud of small drops is readily distinguishable from the strain-confined liquid. We report here on experiments on both stressed and unstressed ultrapure dislocation-free Ge crystals. Where possible, direct comparisons will be made between the γ drop and a cloud of α drops produced in the *same* sample when the stress is removed. The measurements may be grouped into several categories.

a. Spectroscopy of the electron-hole liquid. The recombination luminescence was measured vs wavelength at 1.8 and 4.2 K for various laser excitation levels. The luminescence linewidth from the γ drop is constant at low excitation levels, indicating a constant e-h pair density in the liquid. From these data at intermediate stresses we estimate an equilibrium density $n_\gamma(1.8\text{ K}, -\sigma \approx 6\text{ kgf/mm}^2) = 0.50 \times 10^{17}$ cm^{-3}, compared to the α-drop density $n_\alpha(1.8\text{ K}) = 2.2 \times 10^{17}$ cm^{-3}.[2] Luminescence from excitons in equilibrium with the strain-confined liquid was observed, giving an estimate of the exciton condensation energy, $\phi \approx 1$ meV. Aside from the spectral differences between α and γ drops, the intensity of the γ-drop luminescence was observed to be relatively independent of temperature between 1.8 and 4.2 K, indicating that the strain gradient inhibits boiloff from the liquid. In addition, many of these properties have been studied as a function of stress. Magneto-oscillations in the luminescence intensity were observed which determine an electron Fermi energy in agreement with spectroscopic data. From the luminescence lineshape and the magneto oscillations in luminescence intensity, we find evidence that only one conduction valley is occupied in γ drops.

b. Decay kinetics. Time dependence of the total luminescence yields the volume decay time $\tau_\gamma = 400$ to 600 μsec, compared to $\tau_\alpha = 40$ μsec for α drops at 1.8 K. This enhanced τ_γ is relatively constant below 4.2 K, consistent with a reduced density and inhibited evaporation from the strain-confined liquid. The γ-drop lifetime is found to be greatly reduced in dislocated Ge.

c. Imaging of the recombination luminescence. Time-resolved spatial profiles of γ drops and α clouds are obtained by scanning the crystal image across the spectrometer slit. Taking into account the difference in lifetimes, comparisons can be made between the γ-drop density and the average e-h pair density over the α cloud. The cloud density is two orders of magnitude smaller. Under square-wave modulated excitation, decays of these luminescence profiles have been observed at 1.8 K. The radius of the γ drop decays in time, as expected, whereas the cloud radius does not. Results are in agreement with previous Alfvén wave measurements.[16]

The experimental techniques used in the present study are described in Sec. II. In Sec. III we discuss the spectroscopic properties of γ drop and FE luminescence, including the measurement of the γ-drop density, and exciton condensation energy ϕ. The stress and magnetic field dependences of the luminescence are also discussed. The lifetime and temperature dependences of the luminescence are discussed in Sec. IV. In Sec. V the spatial properties of γ drops and α clouds are compared, including the dependence on the excitation level and on the time after turn off of the excitation source. In Sec. VI the principal results

are summarized and discussed, including the determination that only one conduction valley is occupied in γ drops.

II. EXPERIMENTAL PROCEDURES

The crystals of ultrapure dislocation-free Ge used in these experiments contained $N_A \leq 10^{11}$ cm^{-3} and were grown by Hansen and Haller.[17] The samples were cut along crystal symmetry axes to dimensions $3.85 \times 3.85 \times 1.75$ mm and etched in a $3HNO_3$:HF solution. In most of the experiments below a force was applied along a ⟨111⟩ axis of the crystal, resulting in a single potential well for the EHL; a ⟨110⟩ axis was perpendicular to the 3.85×3.85 mm face [(110) face]. The sample was mounted as in Fig. 1(a), very similar to the arrangement previously used.[4] This arrangement allowed viewing along the (110) face ("face view") as well as along the stress direction via a mirror oriented at 45° below the sample ("end view"). The stress was applied from above by a rounded nylon plunger (contact sphere radius ≈4 mm). The force on the nylon plunger was transmitted by a stainless-steel rod from a calibrated spring arrangement outside the cryostat. Typically, a 10-kgf force was applied to the plunger before cooling the sample. This procedure created a contact area of about 1 mm^2. As described in Sec. III, after the crystal and plunger were cooled to ^{4}He temperatures this contact area remained relatively insensitive to variations in the applied force. The applied force could be varied between 0 and 25 kgf while the sample was immersed in liquid helium. In one experiment described in Sec. III B a slightly rounded brass plunger was used to contact the sample through a thin sheet of mylar. In this case the contact area was found to increase considerably with applied force.

A schematic diagram of the optical system is shown in Fig. 2. Light from the 2-W argon-ion laser was filtered with an H_2O bath to attenuate the infrared radiation from the plasma tube. A special mechanical chopper was built to modulate the laser light: sufficiently fast rise and fall times (≈5 μsec) were obtained by focusing the laser beam to a point in the chopping plane. Typically, square wave modulation at 225 Hz was employed. The laser light was focused to ≃100-μm spot on the Ge surface, accurately positioned by translating the laser focussing lens.

We used a modification[18] of the imaging technique employed by Pokrouskii[2(a)] and Martin[15] to study the spatial distribution of the luminescence emanating from the sample. A precision imaging lens (Fig. 2) formed a sharp, 3× magnified image of the crystal onto the entrance plane of a $\frac{1}{4}$ meter Jarrell-Ash spectrometer. In experiments of Refs.

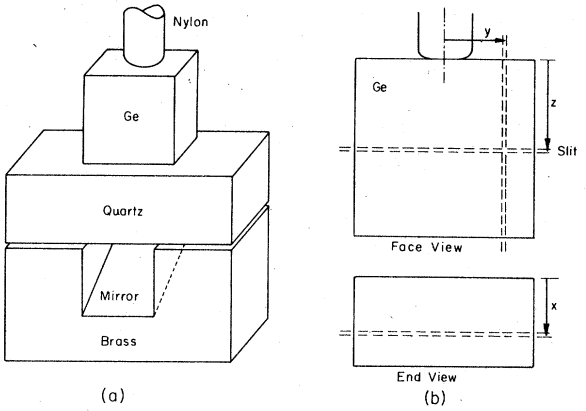

FIG. 1. (a) Method for applying a contact stress to a Ge crystal. The force is applied to the rounded nylon plunger by a calibrated spring arrangement outside the cryostat. (b) Definition of the coordinate system used in this paper. In a "y scan" the image of the crystal is translated across a vertical spectrometer slit. Only the luminescence radiation passing through this slit is detected. In a "z scan," the image of the face view is translated across a horizontal spectrometer slit. In an "x scan," the end view image from the 45° mirror is translated across a horizontal slit.

2(a) and 15, the laser spot was translated across an unstressed Ge sample, thus moving the α-cloud image across the entrance slit of the spectrometer. Because the γ drop remains fixed in the crystal, we have modified this technique as follows: the luminescence image of the entire sample was translated across the front of the spectrometer, using a deflection mirror precisely controlled by stepping motors. A spectrometer slit could be

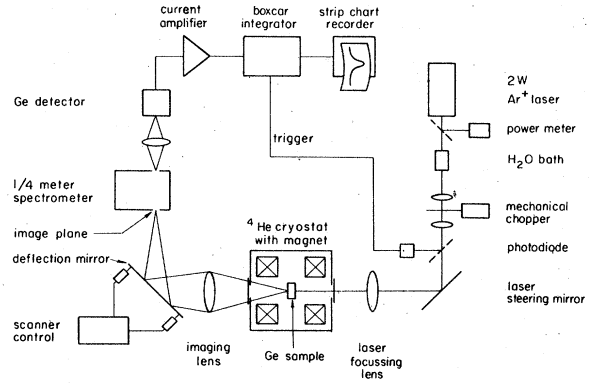

FIG. 2. Schematic plan view of the experimental apparatus. The deflection mirror can be automatically scanned about two axes, vertical and horizontal, thus translating the image of the crystal in the image plane of the spectrometer past a slit oriented either horizontally ("z scan" or "x scan") or vertically ("y scan"); see Fig. 1(b).

mounted vertically or horizontally [Fig. 1(b)], permitting only luminescence from a narrow strip of the crystal to enter the spectrometer. This technique allowed time- and wavelength-resolved image scans to be taken along three orthogonal spatial directions. The following conventions are followed in this paper [Fig. 1(b)]: a "y scan" is formed by translating the image horizontally, across a vertical slit; a "z scan" is formed by translating the *face view* of the image vertically, across a horizontal slit; while an "x scan" is formed by translating an *end view* vertically, across a horizontal slit. The zero point of these scans is as follows: $y=0$ at the center of the crystal (below the plunger); $z=0$ at the face of the crystal contacting the plunger; and $x=0$ at the face of the crystal illuminated by the laser. A scanner control circuit allowed precise digital positioning and recording of the mirror tilt, or image position. The distance the image was translated by one step of the stepper motor was different in the vertical and horizontal directions; these distances were about 12 μm for y scans and 8 μm for z and x scans. The spectrometer allowed wavelength resolution of the luminescence, which was detected by a cooled high-sensitivity Ge photodiode. A PAR model 160 boxcar integrator was used to obtain images at discrete times after turn off of the laser excitation. These delay times ranged from 5 μsec to 2 msec with a time resolution (amplifier rise time and boxcar gate width) of 10 μsec.

The spatial resolution of the luminescence images was determined by the slit width and the sweep speed used for the slit scans, by the resolution of the lens, and by the optical quality of the crystal surface. After the etching procedure described above, the two faces of sample CR38 through which luminescence was collected were polished with Syton. The best resolution we have obtained in this way is estimated to be $\approx$40 μm.

The luminescence profile from a slit scan of a constant-density spherical (or ellipsoidal) object should be

$$I(x) \propto R^2 - x^2 \tag{1}$$

where x is the slit position and R is the radius of the object (γ drop or α cloud). The full width at half maximum W of the profile is related to the radius R by

$$R = W/\sqrt{2}. \tag{2}$$

This relation is true if the slit width is sufficiently small compared to R; in fact, Eq. (2) is true within a few percent if the slit width $s \leq 0.7\ W$. For the case $s = 0.7\ W$ the *shape* of the profile is affected by the finite slit width, but the *width* (full width at half maximum) of the profile is not significantly changed. Equation (2) is used throughout this paper to obtain both γ-drop and α-cloud radii. The slit scans were obtained using standard 250- or 150-μm spectrometer slits, allowing resolution of γ-drop radii $\gtrsim$80 or 50 μm, respectively, due to image magnification. The sweep speed was always chosen so as not to affect the width of the scans.

We used a Tessar 105-mm $f/3.5$ camera lens for high-quality images. The lens was positioned to give the narrowest γ-drop profile at moderately low excitation. It is important to focus using EHL luminescence, since the focal length of the lens changes with wavelength. (The focal length is about 5% longer at 1.75 μm than at 0.5 μm.) The resolution of such a lens is estimated to be <40 μm.

The excitation level is given in this paper by the actual laser power P_{abs} absorbed into the Ge sample. As in Ref. 4, this was obtained by measuring the laser output at various points in the optical path using a thermopile, and checking that there was no significant ir transmitted through the H_2O bath. Our values of P_{abs} include the fact that only 47% of light at 5145 Å is absorbed into Ge at 4 K.[19] In previous publications[16,18,20] the laser output P was given; the absorbed power $P_{abs} \approx 0.3P$.

The luminescence intensity or signal is given in this paper as the output of the current amplifier (Fig. 2), in mV. Although the signal is in general amplified further by other amplifiers or the boxcar, this reference was chosen because it is in principle possible to relate this quantity to the number of photons/sec incident on the detector. However, an absolute measurement of the sensitivity of our detector has not been made.

III. SPECTROSCOPY OF THE RECOMBINATION LUMINESCENCE

In Ref. 4 it was shown that γ drops form in three-dimensional potential wells created by the inhomogeneous strain. The luminescence spectrum is shifted by the strain to lower energy than the spectrum of α-drops in unstressed Ge. Figure 3 shows a complete spectrum for a sample stressed in the ⟨111⟩ direction, showing the TO-, LA-, and TA-assisted phonon replicas. For the applied force of 9 kgf the spectrum is shifted by about 2.5 meV from the α-drop spectrum. In this section we examine the intensity, line shape, and energy of the γ-drop luminescence under various experimental conditions.

A. Liquid-gas phase transition

In order to establish the existence of a liquid-gas phase transition it was necessary to observe

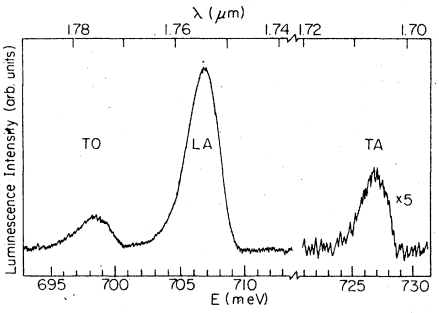

FIG. 3. Luminescence spectrum of a γ drop in Ge at $T=1.8$ K, $P_{abs}=11$ mW and applied force $F=9$ kgf, along $\langle 111 \rangle$, showing the three phonon-assisted lines. The absolute intensities have not been corrected to account for a wavelength-dependent detector sensitivity. Monochromator resolution (full width at half maximum) is 0.66 meV. The shift of about -2.5 meV from the α-drop spectrum corresponds to a stress $\sigma \approx -6.4$ kgf/mm^2, estimated as in Fig. 7. (Compressional stresses are taken to be negative.)

the excitonic gas in equilibrium with the EHL. At 1.8 K the number of FE evaporated from the liquid was not sufficient to observe their radiation. The number of FE was presumably reduced by backflow into the liquid, caused by the stress-induced potential gradient at the liquid surface. Thus to observe the equilibrium excitons it was necessary to raise the temperature and reduce the excitation level, thereby creating a small drop in the shallow

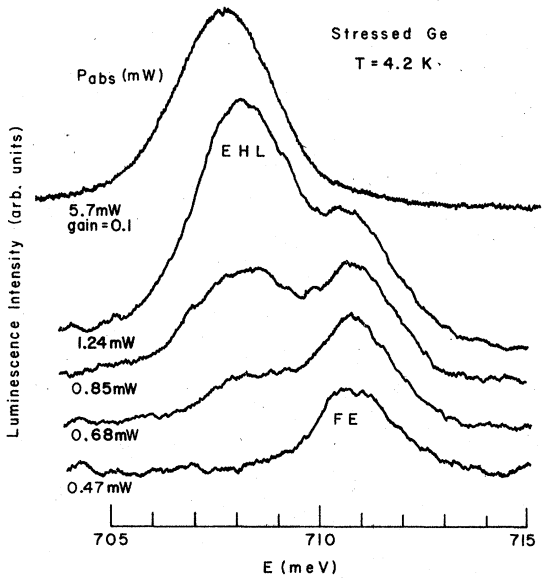

FIG. 4. Luminescence spectra of a stressed Ge sample at 4.2 K, showing both the EHL and FE lines (LA phonon assisted). The stress was approximately -5.5 kgf/mm^2 along $\langle 111 \rangle$. A sharp excitation threshold in the liquid luminescence is observed.

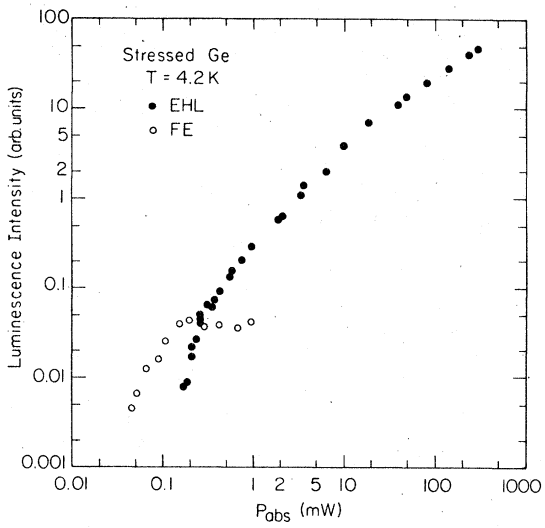

FIG. 5. Dependence of the EHL and FE peak intensities on excitation level, at 4.2 K. A sharp threshold at $P_{abs} \approx 0.15$ mW in the EHL luminescence is observed, characteristic of the gas-liquid phase transition. The pumping efficiency is different from that in Fig. 4 due to a translation of the excitation point.

portion of the strain gradient. Figure 4 shows the luminescence spectra for several excitation levels at 4.2 K, revealing the existence of two distinct spectral lines which are interpreted as the liquid and gas phases. The EHL and FE peaks are closer than in an unstressed sample, indicating a reduced exciton condensation energy.

The onset of the liquid-gas phase transition is clearly observed. At the lowest excitation levels only the exciton luminescence at 710.7 meV is present. As the exciton density is increased a distinct pumping threshold in the EHL luminescence intensity is observed. Figure 5 shows the EHL and FE intensities versus excitation power

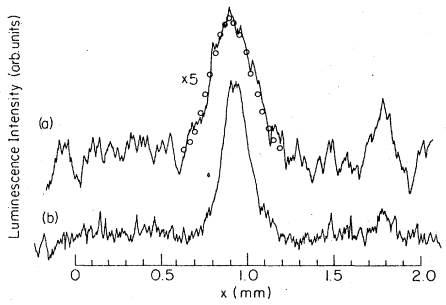

FIG. 6. Spatial luminescence profiles at 4.2 K, showing that the gas and liquid are both in the strain well in the sample. The laser is incident on the face at $x=0$. Spatial resolution ≈ 80 μm. (a) FE gas phase, near threshold. The open circles are Eq. (4) with $\alpha=11$ meV/mm^2. (b) Liquid phase, at a somewhat higher excitation level.

showing that once the nucleation of the liquid phase has occurred, additional e-h pairs added to the system go predominantly into the liquid phase without greatly increasing the number of excitons. A similar threshold phenomenon has been studied extensively[21] for small EHD in unstressed Ge and is a characteristic property of drop nucleation from the saturated gas.

To confirm that both phases occur in the same region of the crystal, luminescence image scans were performed as described in Secs. II and V. Figure 6(a) shows a scan in the x direction for the exciton phase near threshold, and Fig. 6(b) shows a similar scan for the liquid phase at a higher excitation level. It can be seen that both phases are spatially localized in the strain well.

The liquid, which has a higher equilibrium density, is concentrated near the center of the well, whereas the gas occupies the entire well. From the spatial distribution of the excitons, the shape of the strain well can be estimated. By treating the excitons as an ideal gas and setting the chemical potential equal to a constant , the gas density profile is expected to be

$$n(r) = n(0)\exp(-E_s(r)/kT)\,. \tag{3}$$

The strain energy is taken to be parabolic: $E_s(r) = \alpha r^2$, where $r = 0$ is the center of the strain well. It follows that the luminescence intensity in a slit scan is:

$$I(x) = I(x_0)\exp(-\alpha(x - x_0)^2/kT)\,, \tag{4}$$

where x_0 is at the center of the well. The open circles in Fig. 6(a) represent Eq. (4), with $\alpha = 11$ meV/mm^2. This value is in reasonable agreement with the two-dimensional calculation of the EHL energy versus position presented in Ref. 4. Thus the shape of the FE distribution is satisfactorily explained in terms of an ideal gas, at the lattice temperature, in a potential-energy gradient.

Because the FE are localized in the strain well, the effective volume of the gas is smaller than that which can be obtained in unstressed Ge with uniform pumping over a large surface area. Thus the exciton luminescence intensity at threshold is smaller for our inhomogeneously stressed samples, and we have so far observed the free excitons only at temperatures $T \geq 3.3$ K.

From the gas and liquid energy spectra, it is possible to measure the condensation energy ϕ lost by an e-h pair in the gas-liquid transition. It is theoretically expected[6,7,10,22] that ϕ will be smaller in samples under ⟨111⟩ stress than in unstressed Ge. This is evident in Fig. 4, from the greatly reduced separation between the EHL and exciton luminescence lines, as compared to unstressed Ge. However, ϕ cannot be simply measured by the splitting between these two lines: at such high temperatures, the EHL spectrum is broadened even near threshold, due to the enhanced compressibility of the liquid; and at all temperatures, the shape of the FE luminescence line must be corrected for broadening due to the strain gradient. A preliminary value of $\phi \approx 1$ meV has been measured[23] from the EHL and FE luminescence line shapes and separation at a somewhat lower temperature ($T = 3.3$ K), using these modifications of the analysis. A similar value for ϕ was also measured[23] thermodynamically, from the temperature dependence of the exciton density at the threshold for drop formation. A detailed study of the strain-confined e-h fluid phase diagram will be published separately.[24] The value $\phi \approx 1$ meV should be compared with $\phi \approx 2$ meV ($T = 3.5$ K) in unstressed Ge.[25,26]

B. Stress dependence of the luminescence

Figure 7(a) shows the variation of the luminescence peak energy as a function of applied force F. It can be seen that the peak energy shifts linearly with F, above a critical force F_0, similar to experiments on uniformly stressed Ge.[27] However, the origin of the discontinuity in slope is believed to be different in the two experiments.

A ⟨111⟩ uniaxial stress splits the conduction-band degeneracy in Ge, raising three valleys in energy and lowering the fourth. At some critical stress σ_0 this strain splitting becomes equal to the electron Fermi level inside the liquid. At higher stresses only the lowest valley is occupied, and the luminescence peak shifts to lower energies parallel to the shift of this conduction-band edge. At lower stresses, when all four valleys are partly occupied, the luminescence peak position is almost independent of stress, and apparently shifts slightly to higher energies. Only for stresses larger in magnitude than σ_0 are EHD attracted by strain gradients toward regions of higher strain.

In our inhomogeneous stress experiments (Fig. 7), when the applied force is small, the maximum stress σ_M is smaller than σ_0 in magnitude, so that EHD are not attracted to the point of maximum stress; indeed, they may be slightly repelled. For these low applied forces, the luminescence is due not to carriers inside the well, but to small droplets in a cloud near the laser spot. Thus the luminescence peak [Fig. 7(a)] is only weakly shifted by the stress, while the linewidth ΔE (defined as the full width at half maximum of the luminescence spectrum) [Fig. 7(b)] and lifetime τ [Fig. 7(c)] are characteristic of α drops in unstressed Ge.

Once F exceeds some critical value F_0, however, the drops in the cloud are attracted to the stress

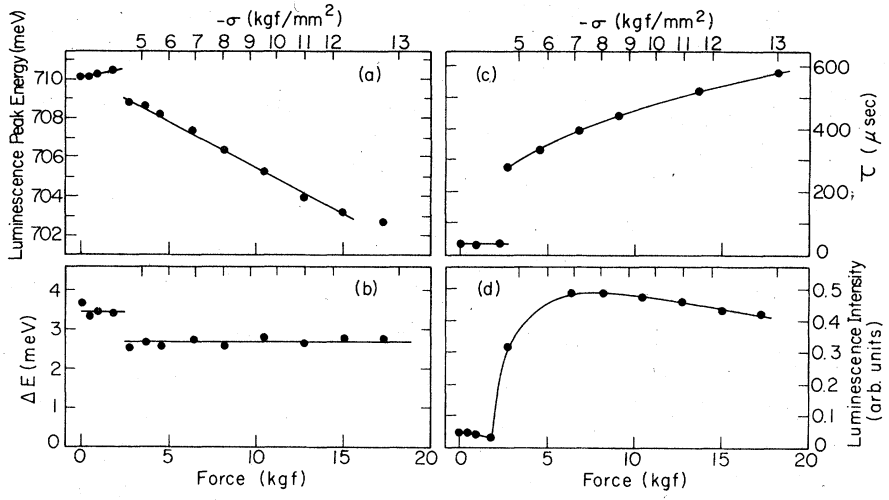

FIG. 7. (a) Luminescence peak energy vs applied force F in kilograms force (kgf), for a sample stressed along ⟨111⟩. The determination of the σ scale is discussed in the text. The γ drop is formed above a threshold force $F_0 \approx 3$ kgf. (b) EHL linewidth ΔE (full width at half maximum) vs applied force. The linewidth is the full width at half maximum of the luminescence spectrum. (c) EHL lifetime τ vs applied force, taken from the tail of the decay curve, as described in Sec. IV. (d) Total luminescence intensity vs applied force. $P_{abs} = 3.2$ mW, $T = 1.8$ K.

maximum, forming a γ drop with very different properties, as seen in Fig. 7. The force F_0 is in general not the same as the force at which $\sigma_M = \sigma_0$, since the cloud of drops is localized near the crystal surface and will not be attracted into the well unless $|\sigma_M|$ is somewhat larger than $|\sigma_0|$. Once small drops are attracted into the well, a γ drop forms, with a greatly enhanced recombination lifetime [Fig. 7(c)] and peak luminescence intensity [Fig. 7(d)], and a reduced linewidth [Fig. 7(b)], all characteristic of a reduced e-h pair density (see discussion in Secs. III C and III D).

For $F > F_0$ the luminescence is due to carriers inside the well, and the stress-dependent properties of γ drops can be studied. The luminescence peak is seen to shift to lower energies approximately linearly with F ($F > F_0$). The magnitude of the strain at the bottom of the well cannot be measured directly,[28] but is estimated from the shift of the γ-drop luminescence peak, assuming that the stress at the bottom of the well is essentially a ⟨111⟩ uniaxial stress. In Ref. 4 this was shown to be a reasonable assumption. Using the peak energy versus uniaxial stress data taken from Ref. 27, the resultant stresses are calculated and shown at the top of Fig. 7.

The changes in the properties of γ drops with stress (for $F > F_0$ in Fig. 7) are not yet very well understood. Theoretically, the γ-drop density is expected to decrease with a large ⟨111⟩ stress,[5-7,10] and this result has recently been observed under uniaxial ⟨111⟩ stress,[29,30] where the luminescence linewidth was seen to decrease with increasing stress. In the strain well there are complications which can make this density change harder to observe. The drop tends to compress,[5,31,32] increasing the average pair density above the equilibrium value. This effect will be discussed in greater detail in Sec. III C. However, the compression should be more significant at higher stresses for two reasons: first, the strain gradient is larger, and second, the compressibility of the drop increases as the equilibrium density decreases. It is clear that the luminescence linewidth, Fig. 7(b), does not decrease as much as in the uniform stress experiment.[29,30] However, the pair recombination time increases with increasing stress [Fig. 7(c)], suggesting a corresponding decrease in pair density, which may be masked in Fig. 7(b) by an inhomogeneous line broadening (see Sec. III C). A quantitative analysis of $n(\sigma)$ and $\tau(\sigma)$ is presently being made, and will be discussed elsewhere. It should be noted that we do not observe the sharp *decrease* in lifetime or intensity which had been reported in earlier uniaxial stress experiments.[33]

In Fig. 7(a) the linear energy shift with applied force suggests that the contact area is relatively constant, unlike the classical Hertzian contact problem.[4,13] An explanation of this is that the nylon plunger undergoes a plastic deformation when the 9-kgf force is initially applied at room temperature. The nylon becomes much stiffer at liquid-helium temperatures and retains the initial contact area for a wide variation in force. This conclusion is supported by birefringence data[4] which show that the position of the strain maximum is only weakly dependent on force.

By contrast, Fig. 8 shows the results of a different experiment, in which the stress was applied through a *metal* plunger. A slightly rounded brass

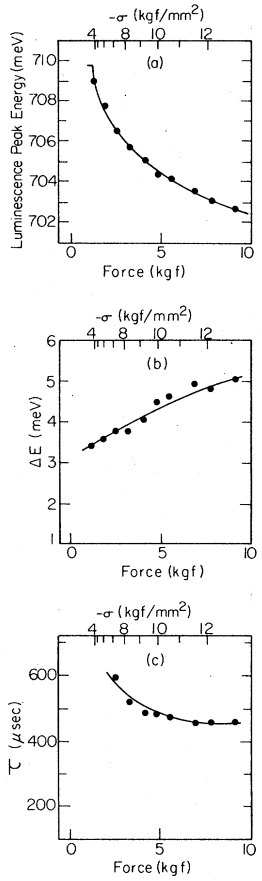

FIG. 8. (a) EHL luminescence peak energy, (b) linewidth ΔE, and (c) decay time τ vs applied force F for a sample stressed along ⟨110⟩. Because the force was applied with a metal rod, the stress was not linearly proportional to the applied force (see text). The solid curve in (a) corresponds to $F^{1/3}$. P_{abs} = 25 mW, T = 1.8 K.

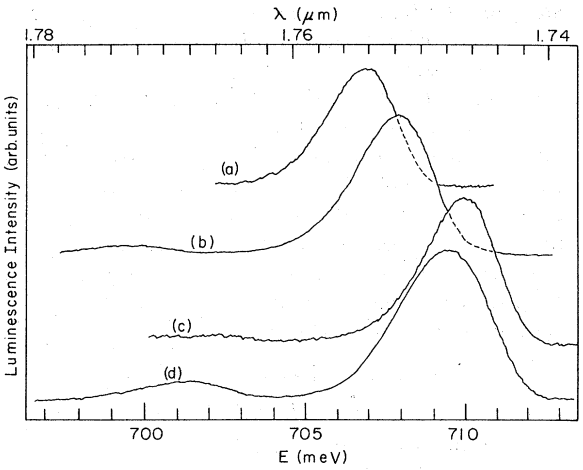

FIG. 9. EHL luminescence spectra from samples with approximately equal applied stresses (permanent stress geometry) and for unstressed Ge. (a) Force parallel to ⟨111⟩. (b) Force parallel to ⟨110⟩. (c) Force parallel to ⟨100⟩. (d) Unstressed Ge.

rod contacted the crystal through a thin sheet of mylar. (The mylar interface reduced the effect of small high stress regions at the contact, caused by surface irregularities.) This case more nearly resembled the classical contact problem: an increase in the contact area with stress was observable in the birefringence, and the maximum stress point moved deeper into the crystal with increasing stress. The brass, being less deformable than nylon, made contact with the Ge over a smaller area A. This caused a larger maximum stress $\sigma_M = F/A$ and strain gradient for a given force, and accordingly a smaller threshold force for the formation of γ drops. Note that the luminescence for $F = 9$ kgf has shifted as much as for $F = 18$ kgf with the nylon plunger. (This is especially significant since the force was here applied along ⟨110⟩; see below.) From the solution of the classical problem of two perfectly elastic contacting spheres, it is expected[13] that $A \propto F^{2/3}$. For this case $\sigma_M \propto F/A \propto F^{1/3}$, which is plotted as the solid curve on Fig. 8(a). In this curve, the point $F = 0$ was shifted to give the best fit. Possible reasons for this shift are: (a) it was difficult in the experiment to determine precisely the point at which the rod first made contact with the crystal; and (b) at liquid-helium temperatures, the mylar interface may have been distorted, giving an apparent minimum value of $A > 0$.

The effects of compression of the liquid are more evident in this metal-plunger experiment: the strain gradient is larger and the drop size is larger due to an increased P_{abs}. The luminescence linewidth [Fig. 8(b)] increases and the lifetime [Fig. 8(c)] decreases with stress, corresponding to an increasing density with stress. Also the total luminescence decay is quite nonexponential, indicating that the density decreases as the drop size decreases.

In Refs. 4 and 11 it was shown that 1, 2, or 4 energy minima for the EHL can be formed by stressing along ⟨111⟩, ⟨110⟩, or ⟨100⟩, respectively. It was found that all of these cases actually correspond to drops forming regions of *local* ⟨111⟩ strain, so that the properties of the strain-confined liquid should be independent of the direction of the applied force. Figure 9 shows a comparison of γ-drop luminescence spectra obtained for approximately equal applied forces along ⟨111⟩, ⟨110⟩, and ⟨100⟩ directions, as well as for α drops in an unstressed sample. [The force is applied via the "permanent" stress geometry as in Fig. 17(a) of Ref. 4.] Because γ drops form in regions of local ⟨111⟩ strain, the energy shift should vary with the projection of a particular ⟨111⟩ axis on the applied force direction. This conclusion is qualitatively verified in Fig. 9 where the shift in the ⟨100⟩ and ⟨110⟩ stressed crystals is considerably less than for ⟨111⟩ stress.[34] The magnitudes of the shifts are approximately in agreement with the predictions of Ref. 4. Note that for all three stressed

samples the luminescence linewidths are similar, and are narrower than the linewidth from the unstressed sample.

Because the properties of the strain-confined EHL are independent of the direction of the applied force, most of our experimental results are for samples stressed along ⟨111⟩, since only a single drop forms. The rest of the paper will deal with the properties of γ drops at (approximately) a fixed value of the stress $|\sigma_M| \simeq 5$–6 kgf/mm^2 corresponding in our experimental arrangement to an applied force $F \approx 9$ kgf.

C. Luminescence linewidth and compression of the strain-confined liquid

Assuming a relatively constant fraction of the photoexcited carriers go into a single γ drop, the properties of the strain-confined liquid can be studied as a function of drop size by simply varying the excitation level. Figure 10 shows the luminescence linewidth ΔE (full width at half maximum of an energy spectrum) plotted versus absorbed laser power P_{abs}. The crystal was stressed along the ⟨111⟩ direction, with $F \approx 9$ kgf and $|\sigma_M| \approx 5$–6 kgf/mm^2, estimated from the energy shift of the luminescence spectrum. At low excitation levels, i.e., for sufficiently small drop size ($P_{abs} \lesssim 5$ mW, $R \lesssim 200$ μm), the linewidth is constant, indicating a constant density within the drop. In this regime the lineshape is used to estimate the e-h pair density, as discussed in Sec. III D. For higher excitation levels, i.e., larger drop size, the linewidth increases with P_{abs}. For comparison, Fig. 10 also shows the linewidth of the luminescence from α drops in unstrained Ge. As anticipated, this width is independent of excitation level.

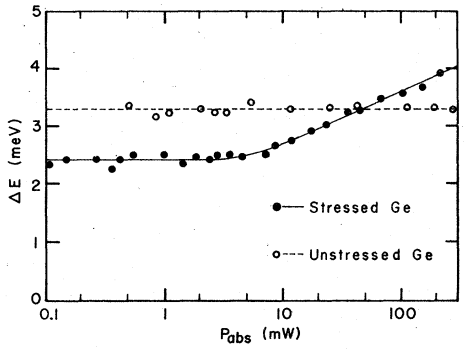

FIG. 10. Comparison of the full width at half maximum linewidths ΔE for the α- and γ-drop LA-assisted lines as a function of excitation level. At low powers both ΔE are constant, as expected for a constant-density liquid phase. At $P_{abs} \gtrsim 5$ mW, corresponding to $R_\gamma \approx 200$ μm, the γ-drop linewidth becomes noticeably broadened by the strain gradient and by compression of the liquid, as explained in the text. $T = 1.8$ K.

Several factors contribute to the power dependence of the γ-drop linewidth. The total luminescence is a superposition of the luminescence from different parts of the drop. Since the magnitude of the stress is a function of position in the well, the luminescence is shifted to higher energies near the surface of the drop, where the magnitude of the stress is lower. From Ref. 4 the strain energy is approximately parabolic, with

$$E_s(r) = \alpha r^2 , \tag{5}$$

measured from the bottom of the well, with $\alpha \approx 8$ meV/mm^2 for our experimental conditions. Thus for a 400-μm radius drop, the luminescence energy would vary by ~1.3 meV across the drop.

Since the strain gradient acts as a restoring force on electrons and holes, a deep potential well also acts to compress the liquid, resulting in an increased pair density and luminescence linewidth.[35] It can be shown[5] that for small variations from the equilibrium density n_0, the density variation within a γ drop is approximately given by

$$n(r) = n_0[1 + \hat{\alpha}(R^2 - r^2)] , \tag{6}$$

where R is the drop radius, $\hat{\alpha} = \alpha/n_0^2 E_0''$ and $E_0'' = (d^2E/dn^2)_{n=n_0}$ is related to the compressibility of the liquid. Vashishta[9] has calculated $n_0^2 E_0'' \approx 0.68$ meV for Ge(1:2) in the zero-stress limit. Thus the density is greatest at the center of the drop and falls to the equilibrium value n_0 at the surface of the drop. According to Eq. (6), for a 400-μm radius drop, we find $n(r=0) \approx 3n_0$. For such a large drop the deviation from the equilibrium density is no longer small and so Eq. (6) must be regarded as only approximate. The density variation across a 100-μm radius drop, however, is only about 10%. Density variations of approximately this form and magnitude have been recently measured by Abel-transform methods.[31] It is clear that such a large compression has an important effect on many properties of the γ drop, and will be discussed in detail elsewhere.[32] In this paper we note several instances where our data show additional evidence of such a compression.

Figure 11 illustrates the effect of the strain inhomogeneity at the highest light levels. Trace (a) is the spectrum from the center of a large drop at fairly high excitation, $P_{abs} = 58$ mW; spectrum (b) is from a small region near the edge of the same drop; and spectrum (c) is from a smaller drop for which $P_{abs} = 1.4$ mW. The narrowest spectrum is from the small drop, where the density and strain are uniform to within 10%. Spectrum (b) represents the liquid near the surface of the drop: Here the luminescence line is still somewhat broadened by the strain gradient over the observed slit aperature. The peak of the luminescence is shifted to

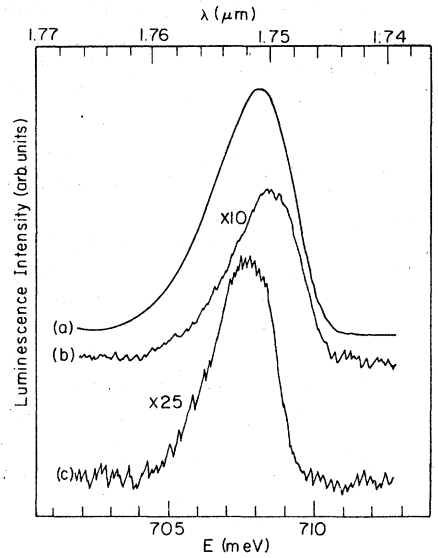

FIG. 11. (a) EHL luminescence spectrum from a slit centered on a large drop, with $R \approx 350$ μm at $P_{abs} = 58$ mW; (b) spectrum from a region near the surface of the same drop; (c) spectrum from a smaller drop with $R \approx 150$ μm, at $P_{abs} = 1.4$ mW. The effective slit resolution on the sample is 80 μm. $T = 1.8$ K.

higher energies, since the local strain is smaller than that at the bottom of the well. Spectrum (a) is a superposition of spectra from liquid at all depths in the well. Spectra (b) and (c) may be used to give another estimate of the strain well parameter α, as follows: since trace (b) was obtained at $r = y \approx 320$ μm (see Sec. II for definition of coordinates), Eq. (5) yields $\alpha \approx 7$ meV/mm^2. This is in reasonable agreement with the estimate in Sec. III A and the prediction in Ref. 4. This data clearly illustrates the role of spatial inhomogeneities in the line broadening at higher excitation levels.

D. Determination of the pair density: Analysis of the luminescence line shape at low excitation

Figure 10 showed that at low excitation levels the luminescence linewidth ΔE, which is a measure of the electron plus hole Fermi energies, is independent of power. This means that for sufficiently small drops ($R \lesssim 150$ μm), the strain is relatively uniform across the drop and the e-h density is constant. This constant density is characteristic of a liquid phase.

The luminescence linewidth of γ drops obtained for $P_{abs} < 5$ mW is actually ≈30% smaller than the linewidth of α drops, measured from the same sample with the stress removed. This occurs in spite of the fact that in stressed Ge the electron degeneracy is reduced. The electron Fermi level depends on the density n as

$$E_F^e \propto (n/\nu)^{2/3}, \tag{7}$$

where ν is the conduction-valley degeneracy. Since the γ drop does not form until the electron degeneracy is removed (ν reduced from 4 to 1), the observed *decrease* in ΔE for the γ drop implies that the density must be considerably lower than in α drops.

Taking into account the change in the hole bands as well, we have determined the equilibrium e-h pair density in a γ drop by fitting the luminescence line shape at low laser pump intensity. As for EHD in unstressed Ge, the luminescence intensity for the LA phonon-assisted line is taken to be[36,37]

$$I(\nu) \propto \iint D_e D_h f_e f_h \delta(E_g + E_e + E_h - \hbar\omega_{ph} - h\nu) dE_e dE_h, \tag{8}$$

where D_e and D_h are the electron and hole density of states, f_e and f_h are the respective Fermi distribution functions, E_g is the energy of the indirect gap, and $\hbar\omega_{ph}$ is the energy of the phonon emitted along with the photon. The electron density of states is that of a single parabolic band

$$D_e(E) \propto m_{de}^{3/2} E^{1/2}, \tag{9}$$

where $m_{de} = (m_t^2 m_l)^{1/3} = 0.22 m_0$ is the electron density-of-states mass. The hole density of states is written in the same form, but in strained Ge the hole density-of-states mass is energy dependent. For one hole band, the mass is given by

$$m_{d\,hh}^{3/2}(E_{hh}) = \frac{\hbar^3}{\sqrt{2E_{hh}}} \int k^2 \frac{dk}{dE_{hh}} \frac{d\Omega}{4\pi}. \tag{10}$$

The dispersion in the strained hole band, $E_{hh}(\vec{k})$, is given in Ref. 38. The above expression is for the "heavy" hole band (the band which remains populated under large ⟨111⟩ compression). A similar expression holds for the "light" hole band when it is populated. The masses $m_{d\,hh}$, $m_{d\,lh}$ were calculated by numerically integrating Eq. (10)—a plot of these masses as a function of reduced energy $E' = E/|\sigma_{111}|$ is given in Fig. 12. The net luminescence is the sum of separate contributions of the form of Eq. (8) for each hole band. We have used Hensel and Suzuki's values[39] for the hole mass parameters and deformation potentials. Stiffness tensor elements are from Ref. 40. The curves of Fig. 12 can easily be fitted with analytic formulas. By using reduced units, the masses may readily be converted to the appropriate value for any stress. In Fig. 13(a) the solid curve is a typical luminescence line shape calculated using this nonparabolic hole band ($-\sigma = 5.6$ kgf/mm^2, $T = 1.8$ K, $n = 0.5 \times 10^{17}$ cm^{-3}). By comparison, the dashed curve is the line shape for a constant hole

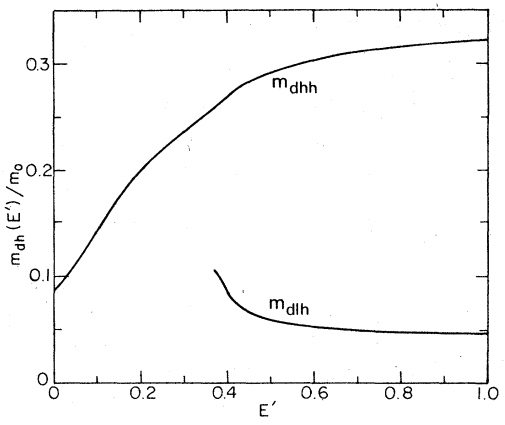

FIG. 12. Heavy and light hole density-of-states masses vs reduced energy $E' = E/|\sigma_{111}|$ with E in meV and σ_{111} in kgf/mm^2. The masses are calculated by integrating numerically over the strain-split bands, as described in the text.

mass $m_{dh} = m_{dhh}(E_F^h)$, using $E_F^h = 2.28$ meV obtained from the previous case. As can be seen from Fig. 13(a), in order to quantitatively analyze the experimental line shapes, the nonparabolic hole masses must be used.

Figure 13(b) shows a fit of the LA phonon-assisted luminescence line for $P_{abs} = 0.17$ mW,[41] $-\sigma_M = 6.8$ kgf/mm^2, and $T = 2.0$ K. The theoretical points are for a density of $n = 0.50 \times 10^{17}$ cm^{-3}. By analyzing several lines, we find

$$n_\gamma = (0.50 \pm 0.05) \times 10^{17} \text{ cm}^{-3} \quad (T = 1.8\text{–}2.0 \text{ K}, \quad -\sigma_M = 5\text{–}7 \text{ kgf/mm}^2). \tag{11}$$

Vashishta[9] has calculated $n = 0.69 \times 10^{17}$ cm^{-3} at

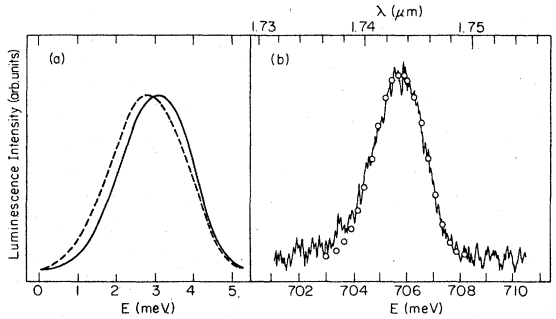

FIG. 13. (a) Theoretical luminescence line shapes. Solid curve: $\sigma = -5.6$ kgf/mm^2, $T = 1.8$ K, $n = 0.5 \times 10^{17}$ cm^{-3} using the nonparabolic masses from Fig. 12. Dashed curve: uses single mass $m_{dh} = m_{dhh}(E_F^h)$, using $E_F^h = 2.28$ meV from the previous case. (b) Experimental luminescence spectrum for a sample stressed in the ⟨111⟩ direction. The stress is $\sigma \approx -6.8$ kgf/mm^2 from the shift of the peak energy. $P_{abs} \approx 0.17$ mW, $T = 2.0$ K. The open circles are the theoretical line shape for nonparabolic masses, $\sigma = -6.8$ kgf/mm^2, $n = 0.50 \times 10^{17}$ cm^{-3}, $T = 2.0$ K.

$T = 0$ for Ge(1:2) in the zero-stress limit, that is with only one conduction valley occupied but with the zero-stress hole masses. Model 1 of Ref. 5 gives a theoretical value of $n = 0.44 \times 10^{17}$ cm^{-3} at $T = 0$ and $-\sigma = 6.8$ kgf/mm^2. Other experimental measurements of the density are discussed in Sec. III E. The overall agreement between experiment and theory is good.

The low-energy tail in Fig. 13(b) is present in all of our spectra, and is more pronounced than the tail observed in unstressed Ge. In unstressed Ge, this tail has been interpreted as partly due to Auger processes modifying the recombination energies of carriers deep inside the Fermi sea.[42] Also, an additional contribution may arise from a "forbidden" luminescence line associated with LO phonons.[43] It is not unlikely that the magnitude of either effect could be enhanced in γ drops.

E. Other methods of estimating the pair density

In a magnetic field, the carrier energy is quantized into Landau levels, and many properties of the carriers have a quasisinusoidal modulation with period $\propto 1/H$. That is, the property undergoes a change whenever $(j + 1/2)\hbar\omega_c = E_F$, where $\omega_c = eH/m_c^* c$ is the cyclotron frequency, m_c^* is the cyclotron mass of the carrier, and j is an integer. In experiments on α drops in unstrained Ge, periodic oscillations have been observed in the luminescence intensity[44] and far-infrared absorption[45,46] and emission.[45] There should be separate sets of oscillations due to electrons and holes, but so far only oscillations due to electrons have been resolved.[47] Similar magneto-oscillatory effects are expected for properties of γ drops.

We have observed magneto-oscillations in the luminescence intensity of γ drops. As in Ref. 44, these oscillations are apparently due to oscillations in pair recombination time τ_0 since the effect became more pronounced as the drop decayed. In these experiments the oscillations in the luminescence intensity were observed by two methods. The first method used a boxcar integrator to observe the total luminescence intensity at discrete times after the light source was shut off. The second method used a phase-sensitive lock-in amplifier to observe the oscillations. Because the luminescence decay time $\tau_\gamma \approx 500$ μsec (see Sec. V A) was comparable to the time the square-wave chopped light source was switched off ($t' \sim 2$ msec), a change in τ_γ shifted the phase of the luminescence signal relative to a reference signal from the light chopper.

At zero field the phase of the reference signal was adjusted to be 90° out of phase with the luminescence signal, corresponding to zero output from

the phase-sensitive lock-in amplifier. Thus the output signal of the lock-in amplifier was sensitive to changes in the luminescence decay time as the magnetic field was increased. This technique has two advantages: first, it utilizes the superior averaging of a lock-in amplifier, and second, the output is not directly affected by small changes in luminesce intensity which are not related to changes in the decay time.[48]

Both techniques yielded oscillations with the same period and phase. Figure 14 shows three sets of oscillations for a sample stressed along ⟨111⟩, for different orientations of the magnetic field with respect to the crystal axes. Trace (a), $\vec{H} \| \langle 001 \rangle$, and trace (b), $\vec{H} \| \langle 110 \rangle$, were taken for $P_{abs} = 3.2$ mW, using the second technique described above. Trace (c), $\vec{H} \| \langle 111 \rangle$, was taken for $P_{abs} = 2.4$ mW at a time $t = 800$ μsec after the light was shut off, using the first technique described above. The period of the oscillations changed consistently with the angular variation in the electron cyclotron mass, assuming the electron masses are unchanged from bulk Ge.[49] These curves were fit using a magneto-oscillatory expression similar to that reported by Keldysh and Silin.[50] It was assumed that only one electron valley was occupied and that the oscillations were due to the electrons and not the holes. From these fits we find the electron Fermi level to be $E_F^e = 2.3 \pm 0.12$ meV ($T = 1.6$ K). This yields an average value for the e-h pair density

$$n_\gamma = (0.52 \pm 0.05) \times 10^{17} \text{ cm}^{-3} \quad (T = 1.6 \text{ K}, \ -\sigma_M \approx 6 \text{ kgf/mm}^2). \tag{12}$$

The above result was obtained at a sufficiently low excitation level that the luminescence linewidth (see Fig. 10) was not broadened, so we consider the above density to be the equilibrium value. At higher excitation levels the period of the oscillations was observed to increase with P_{abs}, indicating compression of the liquid. Figure 15 shows a magnetic field sweep for the same field orientation as in Fig. 14(c) but taken at a much higher excitation level, $P_{abs} = 120$ mW, $t = 100$ μsec. For this data we found $E_F^e = 3.68$ meV, corresponding to $n = 1.05 \times 10^{17}$ cm^{-3}. It is perhaps surprising that, with such a wide range of density within the drop, the oscillations are still very well resolved. While this represents some kind of an average density, it shows clearly that significant compression can easily be obtained with moderate excitation levels.

Ohyama, Hansen, and Turney[51] observed oscillations in the attenuation of longitudinal ultrasound by γ drops in a magnetic field. These oscillations should have the same period as the oscillations in luminescence intensity. From the period of the oscillations they derived the electron Fermi level and hence the density inside the γ drop. The density they obtained was $n_\gamma = (0.62 \pm 0.04) \times 10^{17}$ cm^{-3} ($T = 1.8$ K). However, they were using moderately high excitation ($P_{abs} \approx 20$–40 mW), so that compressional effects should have been significant, explaining the higher value. Indeed, they found[52] that the period of the oscillations varied with P.

The pair density has also been estimated from Alfvén resonances[11,16,18,20,53] in the microwave absorption of γ drops. Standing electromagnetic waves are set up inside the drop, and a resonant absorption occurs when the Alfvén wavelength approximately matches the drop diameter. The resonant magnetic field should provide a measure of the quantity $n_\gamma R^2$. Determining R from a simultaneous imaging experiment, these data imply $n_\gamma \simeq 0.7 \times 10^{17}$ cm^{-3} ($T = 1.8$ K).[54] This represents some kind of an average value, since the depen-

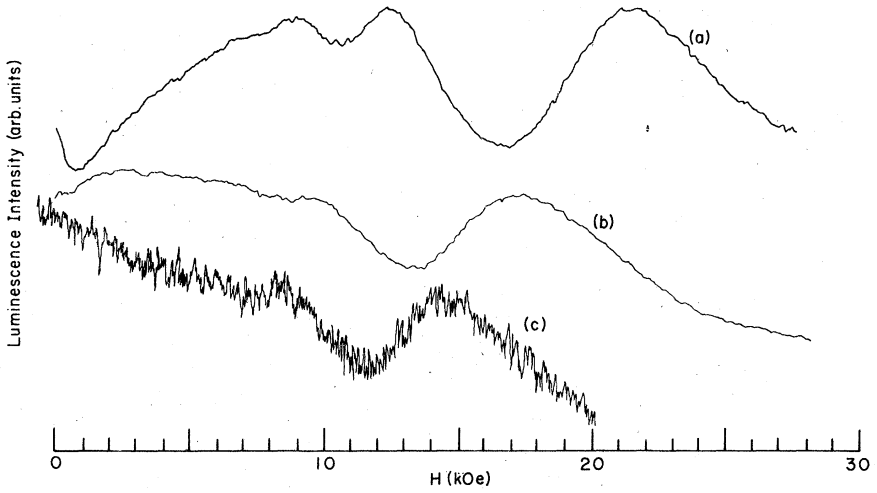

FIG. 14. Total luminescence intensity as a function of magnetic field for three different orientations of the field with respect to the crystal axes. (a) $\vec{H} \| \langle 001 \rangle$, (b) $\vec{H} \| \langle 110 \rangle$ for $P_{abs} = 3.2$ mW, at steady state, (c) $\vec{H} \| \langle 111 \rangle$, for $P_{abs} = 2.4$ mW and $t = 800$ μsec. Permanent stress geometry (stress along ⟨111⟩). $T = 1.6$ K. The vertical scale is offset from zero by an arbitrary amount. The oscillations are about a 10% effect.

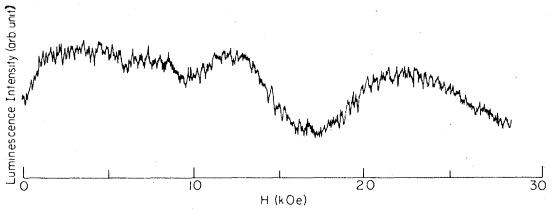

FIG. 15. Total luminescence intensity as a function of magnetic field for the same conditions as for Fig. 14(c), except that $P_{abs}=120$ mW, $t=100$ μsec. The peaks have moved to higher fields, showing compression of the liquid. The vertical scale is offset from zero by an arbitrary amount.

dence of n on drop size was not considered in the analysis. As such it is in reasonable agreement with the Ohyama, *et al.*[51] estimate. However, the analysis is complicated since the theory has only been done for spherical drop shape, while the γ drop becomes markedly nonspherical in a magnetic field.[54-58]

The γ-drop density has also been estimated from experiments on absorption of 3.39-μm infrared light.[59-61] The densities quoted are higher than those observed in other experiments: Pokrovskii and Svistunova[59,60] find $n_\gamma \simeq 1\times10^{17}$ cm^{-3}; Mattos *et al.*[61] find $n_\gamma \simeq 2\times10^{17}$ cm^{-3}. However, the results rely on an absolute measure of the hole interband absorption cross section σ_a at 3.39 μm, and the two authors disagree on the appropriate value to use.[62] (It is even possible that this cross section changes with stress.) Until this point is clarified, it is difficult to know the accuracy of these results. It should be noted that the drops observed in Refs. 59 and 60 were large enough that there could have been some compression, and apparently the stress was not determined.

Finally, the pair density was measured by Aurbach *et al.*[63] from observation of far-infrared plasma absorption. This experiment yielded $n_\gamma \simeq 4\times10^{16}$ cm^{-3} for $F\approx9$ kgf. The size of the drop could not be readily determined, although the peak position of the ir absorption did not shift significantly when the power was reduced by an order of magnitude, suggesting $n\approx$ const. No correction was made for additional absorption due to transitions between the two hole bands.[64-69] Consequently, this value may require some modification.

IV. DECAY KINETICS AND TEMPERATURE DEPENDENCE OF THE EHL LUMINESCENCE

A. Enhanced lifetime of γ drops

The lifetime of the liquid phase is governed by several processes: (i) direct radiative recombination of electrons and holes; (ii) (nonradiative) Auger recombination of an e-h pair, whereby kinetic energy is given to other carriers; (iii) nonradiative recombination due to impurities or lattice defects; and (iv) evaporation of FE or carriers from the surface of the EHL. In unstressed Ge, surface evaporation has been observed above about 2 K and is characterized by a nonexponential decay and a cutoff time; below this temperature the volume decay mechanisms usually predominate The α-drop lifetime is unchanged in samples containing a density of up to 10^{15} cm^{-3} impurity atoms,[70] or up to ~10^3 cm^{-2} dislocations.[71] Since our samples are ultrapure and dislocation free, the impurity and defect contributions to the e-h pair recombination time will be neglected here.

An important difference exists between the radiative and Auger processes. The two-particle radiative recombination rate depends linearly on the e-h pair density n of the liquid phase, whereas an Auger rate depends on higher powers of n. Thus a reduced e-h pair density in the liquid, obtained for example by stressing the crystal, would diminish the Auger contribution to the total recombination rate much more than the radiative contribution. For unstressed Ge, estimates of the ratio of nonradiative to radiative decay rate range from 4 to 0.25.[44b,72-74]

Figure 16(c) shows the decay of the total EHD luminescence for our unstressed sample after the light is switched off. The α-droplet lifetime at 1.8 K was found to be 36 μsec for this sample, in good agreement with published values.[27,75-77]

Figures 16(a) and 16(b) show the much longer decay times characteristic of γ drops. At low excitation levels [Fig. 16(a), $P_{abs}=1.1$ mW] the decay is exponential, with $\tau\approx530$ μsec. At higher excitation levels [Fig. 16(b), $P_{abs}=119$ mW] the decay is noticeably nonexponential. This nonexponential decay is exactly what would be expected for a compressed drop: initially, when the drop is larger, the decay is faster—suggesting a high average pair density. As the drop shrinks, the compression decreases and the instantaneous decay rate becomes slower. For very long delay times, the decay typically becomes exponential, with a time constant comparable to that found in Fig. 16(a) for smaller drop size. Figure 17 shows the change of initial decay time τ_i with pumping power. If the decay were purely radiative ($\tau\propto n^{-1}$), such a change in τ would suggest that the average density is approximately doubled in the largest drops ($R=400$ μm). For smaller drop sizes the density becomes uniform and τ_i approaches an equilibrium value. This value is somewhat sample dependent, but $\tau_\gamma\approx550$ μsec as shown in Fig. 17 is typical.

A simplified model for the enhanced equilibrium

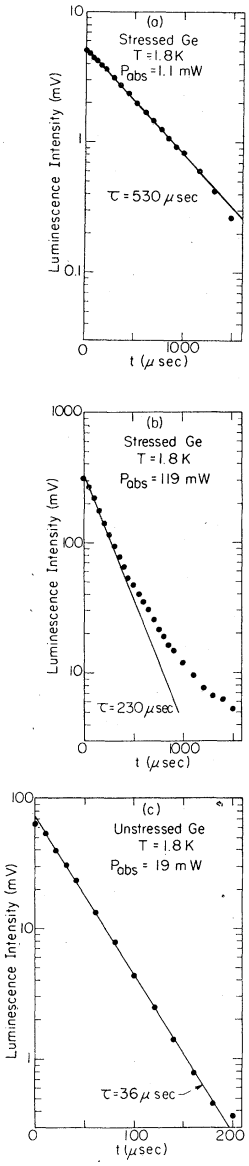

FIG. 16. (a) EHL luminescence intensity as a function of time after the light source is switched off, for a sample stressed along ⟨111⟩, (F = 9 kgf) for P_{abs} = 1.1 mW. (b) Same as (a), with P_{abs} = 119 mW. (c) α-drop luminescence intensity vs time for the same sample after the stress is removed, for P_{abs} = 19 mW. T = 1.8 K.

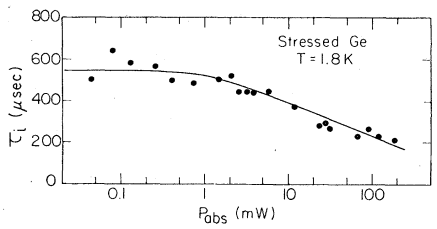

FIG. 17. Initial decay time τ_i as a function of absorbed power P_{abs} for the same sample and strain configuration as in Figs. 16(a) and 16(b).

γ-drop lifetime may be given as follows: the volume decay rate due to radiative and nonradiative processes is

$$\tau^{-1} = \tau_r^{-1} + \tau_A^{-1} = an + bn^s , \tag{13}$$

where a and b are constants and $s = 2$ or greater, depending on the dominant type of Auger process. For α drops we use $\tau_\alpha = 40$ μsec, and $n_\alpha = 2.2 \times 10^{17}$ cm^{-3} and the radiative efficiency $\epsilon_{\text{rad}\,\alpha} = \tau_r^{-1}/(\tau_r^{-1} + \tau_A^{-1}) \approx 0.3$, estimated by Pokrovskii,[78] to determine the constants a and b. The predicted γ-drop lifetime may then be calculated using $n_\gamma = 0.50 \times 10^{17}$ cm^{-3} from the spectral line shape, Eq. (11). For $s = 2$ we predict $\tau_\gamma = 380$ μsec and a radiative efficiency $\epsilon_{\text{rad}\,\gamma} = 65\%$. For $s = 3$ we find $\tau_\gamma = 520$ μsec and $\epsilon_{\text{rad}\,\gamma} = 90\%$. In the latter case, even an unusually large value for the α-drop radiative efficiency $\epsilon_{\text{rad}\,\alpha} = 0.6$ would predict an enhanced γ-drop lifetime, $\tau_\gamma = 255$ μsec. Thus the measured γ-drop lifetimes are in quantitative agreement with those obtained from this simplified equation for τ. Also, this analysis shows that the radiative efficiency of γ drops is considerably higher than for α drops.

A more detailed theory would have to take into account the stress dependence of the coefficients a and b. Physically the energetics of the EHL are modified under reduced degeneracy, and this would affect the enhancement factor ρ, which is a measure of the spatial e-h correlation. The coefficient a should depend linearly on ρ. The stress dependence of the Auger coefficient b is an interesting theoretical problem which has not been solved. Vashishta[9,79] has calculated $\rho_\alpha = 2.3$ for Ge(4:2) and $\rho_\gamma = 3.4$ for Ge(1:2). Assuming the form $\tau^{-1} = a_0 \rho n + b_0 n^s$, where now a_0 and b_0 are independent of stress, and using the same values for $\epsilon_{\text{rad}\,\alpha}$, n_α, and n_γ given above, we find $\tau_\gamma = 370$ μsec with $s = 3$ and $\tau_\gamma = 290$ μsec with $s = 2$. The long observed lifetimes are consistent with the interpretation of a reduced density in γ drops. A more exact comparison must await a theoretical model for the Auger recombination times in stressed and unstressed Ge.

B. Temperature dependence of the luminescence

So far we have concentrated on results for samples in superfluid liquid ^{4}He ($T \approx 1.8$ K). At higher temperatures, the α-drop lifetime is considerably shortened due to boiloff of excitons.[75] For γ drops the effects of boiloff are greatly reduced by the strain gradient: an exciton which boils off the surface of the γ drop will be pulled by the strain back into the drop in a time short compared to the exciton recombination time.[11] The force on an exciton due to the strain gradient is approximately $\vec{F} = -2\alpha\vec{r}$, where α is the strain parameter of Eq. (5). The exciton thermal velocity $v_T = (3kT/m_x)^{1/2} \approx 6.4 \times 10^6$ cm/sec at $T = 4.2$ K, since $m_x = 0.05\, m_0$. If an exciton evaporates from a γ drop of radius $R = 100$ μm and moves radially away

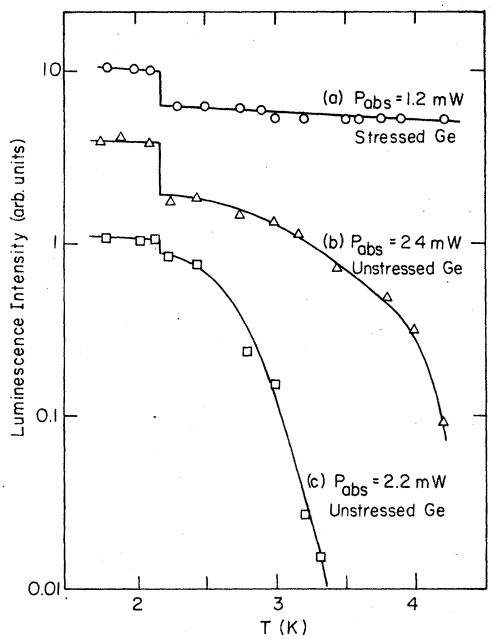

FIG. 18. Luminescence intensity vs temperature. (a) γ drop in a $\langle 111 \rangle$ stressed sample, $P_{abs} = 1.2$ mW. (b) α drops in the same sample after the stress was removed, $P_{abs} = 24$ mW. (c) same as (b), except $P_{abs} = 2.2$ mW. Directly above the λ point of liquid helium, 2.17 K, the luminescence intensity is reduced, apparently due to light scattering by helium bubbles.

at the thermal velocity v_T, then it will be accelerated back into the drop in 0.02 μsec, or less than 1% of its lifetime, assuming $\alpha \approx 8$ meV/mm^2. Thus, even at 4.2 K, shortening of the γ-drop lifetime due to boiloff of excitons is greatly inhibited. This explains the very small number of FE observed in the well even at 4.2 K (see Sec. III A). Figure 18 shows the luminescence intensity versus temperature for γ drops and for α drops at two different light levels. The γ-drop signal is relatively independent of temperature, while the α-drop signal is strongly temperature dependent, due to boiloff.

Figure 19 shows the initial decay time τ_i as a function of excitation level at 4.2 K, for the same $\langle 111 \rangle$ stressed sample as in Fig. 17. The shorter initial time at higher excitation levels is evidence of compression. The lifetime is longer at 4.2 K at all powers than at 1.8 K (Fig. 17) and it levels off to around 670 μsec for small drop size. This increase in lifetime may possibly be explained by a decrease in the γ-drop equilibrium density at higher temperatures,[80] analogous to the temperature dependence of the density in α drops.[81,82]

The lifetime of γ drops at 4.2 K depends sensitively on the details of the strain well configuration. For lower applied forces the decay time becomes shorter: in the sample of Figs. 17 and 19,

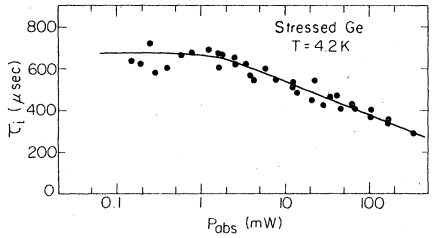

FIG. 19. Initial luminescence decay time τ_i as a function of absorbed power P_{abs} for the same sample as in Fig. 17, with $T = 4.2$ K.

at half the stress, the decay is nonexponential, qualitatively having the characteristic $I(t)$ dependence for boiloff-limited lifetime.[75] For crystals stressed along a $\langle 100 \rangle$ direction, the strain well is usually quite shallow, and strongly temperature-dependent lifetimes have been observed.[63]

V. LUMINESCENCE PROFILES

The spatial position, size, and shape of a γ drop in Ge is observed most directly by a vidicon image[83] of the recombination luminescence. In Fig. 20, we show a photograph of a γ drop produced in a $\langle 111 \rangle$ stressed sample. At a low excitation level an approximately spherical mass of liquid is formed in the bottom of the potential well. At the higher excitation level corresponding to Fig. 20, the increased volume of e-h liquid fills a larger portion of the strain well, displaying a nonspherical shape. For typical values of the liquid surface tension ($\sigma_s \approx 10^{-4}$ erg/cm^2)[84] and strain parameter ($\alpha \approx 8$ meV/mm^2), the strain and surface energies are equal when the drop radius $R \approx 30$ μm. Since the strain energy increases as R^5, while the surface energy increases only as R^2, for large drops the strain energy dominates. Consequently the drop

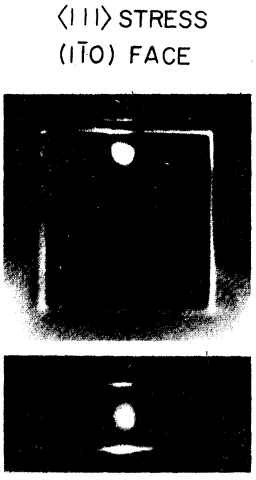

FIG. 20. Luminescence image from a sample stressed in the $\langle 111 \rangle$ direction, viewed through a (110) face and displayed using an infrared vidicon and standard TV monitor. Lower photo is an end view through a (111) face, as shown in Fig. 1(b). The crystal face pumped by the laser is uppermost in the end view. $P_{abs} = 90$ mW, $T = 1.8$ K.

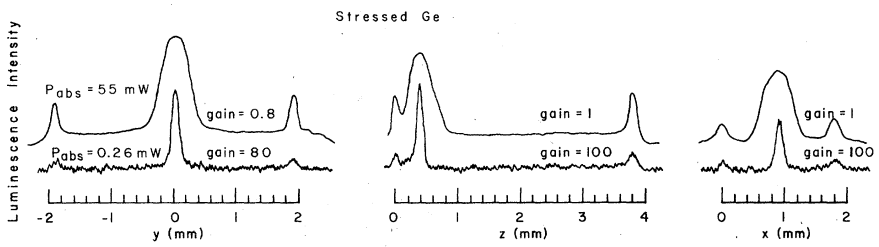

FIG. 21. Luminescence profiles at two different excitation levels for a sample stressed along ⟨111⟩. The small peaks, e.g., at $y \approx \pm 1.9$ mm, are due to scattered light from the edges of the crystal. The upper row of scans is for $P_{abs} = 55$ mW; the lower row is for $P_{abs} = 0.26$ mW. $T = 1.8$ K.

shape conforms to a surface of constant strain energy.

A more quantitative measurement of the luminescence intensity as a function of position in the sample is obtained by the slit-scanning method described in Sec. II. This technique also permits a time-resolved observation of the luminescence profile after the excitation is switched off.

A. Spatial profiles of γ drops

Figure 21 shows a set of γ-drop image scans at two different laser power levels. These slit scans, obtained with 80-μm spatial resolution, clearly show a large increase in the volume of the EHL as the excitation is increased. The boundaries of the crystal are well defined by scattered luminescence light.

The drop radius is plotted versus absorbed laser power P_{abs} in Fig. 22, using Eq. (2) to obtain R from the full width at half maximum of a slit scan. For constant e-h pair density and laser production efficiency the simplest model would predict that the drop volume is proportional to P_{abs}, or $R \propto P_{abs}^{1/3}$. The measured R deviate from the simple $P_{abs}^{1/3}$ power dependence at both the highest and lowest excitation levels. The apparent leveling off of the drop radius at low laser levels is likely due to the finite slit width and the irregular etched surface of the sample, which limit the resolution. (From Alfvén resonances on a similar sample, the radius was measured down to ~30μm.) It is observed that the drop is not spherical, i.e., $R_x \approx R_y \gtrsim R_z$, reflecting the anisotropy of the strain well.

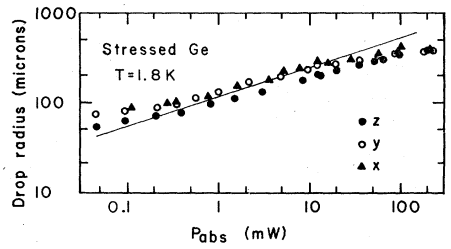

FIG. 22. γ-drop radii vs absorbed power P_{abs} for a ⟨111⟩-stressed sample. The effective spatial resolution was 80 μm, which equals the slit width divided by the image magnification. The solid line has a slope of $\frac{1}{3}$.

In order to observe the total luminescence from the whole drop without spatial selection, we measured the EHL luminescence intensity with no slits in place. This "total" luminescence intensity is plotted as a function of absorbed laser power in Fig. 23, which shows that the total intensity varies approximately linearly with P_{abs} over nearly three orders of magnitude. This is expected for the case where the production efficiency ϵ_{prod} (the number of e-h pairs in the drop per photon absorbed) and the radiative efficiency ϵ_{rad} (the fraction of pairs which decay radiatively) are constant. For constant ϵ_{prod}, the number of e-h pairs in the drop is simply proportional to P_{abs}. Since, from Fig. 22 at $P_{abs} \gtrsim 10$ mW the volume of the drop ($V \sim R_x R_y R_z$)

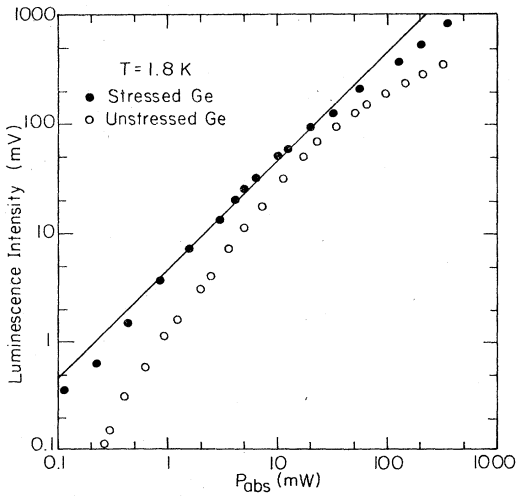

FIG. 23. Integrated luminescence intensity vs absorbed power for the same sample as in Figs. 21 and 22 (●), and for the same sample after the stress is removed (○). The solid line has a slope of 1. The relative intensities of the two sets of data cannot be directly compared due to a change in detector sensitivity between the two runs.

increases much more slowly than P_{abs}, we conclude that the density of the drop at high excitation increases with excitation level. This is further evidence that the liquid is compressed by the strain well for $R \gtrsim 150$ μm, and is consistent with the increased luminescence linewidth, reduced lifetime, and shifted magneto-oscillations observed at higher P_{abs}. For comparison, Fig. 23 also shows the total EHL luminescence intensity for the same crystal after the stress was removed; this represents the total luminescence intensity from a cloud of α drops. The deviations from linearity are undoubtedly due to the complex mechanisms of cloud formation.

An estimate of the e-h pair production efficiency can be made as follows: For a steady-state experiment the number of e-h pairs in the drop is given by

$$N = \bar{n}V = P_{abs}\tau_i \epsilon_{prod}/E_{ph}, \quad (14)$$

where $\bar{n}$ is the average pair density, V is the drop volume, E_{ph} is the energy per photon of laser light, and τ_i is the initial decay time of the drop. For $P_{abs} \lesssim 5$ mW the density was found to be 0.50×10^{17} cm^{-3} from the line shape analysis, as discussed in Sec. III D. We find $\epsilon_{prod} \approx 30\% \pm 10\%$. In the above experiment the laser was focused to a point close to the strain well. The value of ϵ_{prod} decreases as the laser spot is moved further from this position or if the beam is significantly defocused.

B. Comparison with clouds of α drops

The results for unstressed samples are considerably different. Previous experiments have shown that a cloud of small drops (each with radius 1–10 μm) is formed,[14,15,85,86] for point excitation. The average density of e-h pairs in the cloud has been estimated by light scattering to be $\sim 10^{15}$ cm^{-3}, indicating ~1% filling factor of EHD.[14] The cloud radius increases with increasing excitation level, contrary to a simple model of EHD or FE diffusion into the crystal. The details of the cloud formation are not presently well understood, although it has been suggested that drops may be ballistically driven from the excitation point, possibly pushed by a phonon wind.[87–90]

Figure 24 shows a set of slit scans for the same sample before and after the stress is removed, for $P_{abs} = 2.8$ mW. The α-cloud peak intensity is much lower, and the size of the profile is significantly larger, than for the γ drop, indicating a much lower average density of e-h pairs in the cloud than in the γ drop. For the stressed samples, the largest drop was always obtained when the laser was focused near the strain well. For the scans taken after the stress was removed, the laser spot was translated to a position near the center of the pumped face of the crystal.

Luminescence profiles for the cloud in the unstressed sample are shown in Fig. 25, for three different laser intensities. At low and moderate P_{abs} the cloud has a fairly well-defined surface. At high light levels, however, the cloud seems to nearly fill the crystal. (The "lumps" on the slit scans are in part due to imperfections on the crystal face.) At the highest power levels an interesting new phenomenon is observed, as shown in Fig. 26. The three x scans show that as the power is increased, the droplets are forced away from the pumped surface at $x = 0$, perhaps due to heating around the point of excitation. (Note that the experiment is done with cw pumping.) Figure 27 shows a luminescence profile at a moderate excitation level, $P_{abs} = 11$ mW, under increased spatial resolution. The peak of the distribution is distinctly separate from the edge effect peak at $x = 0$. This result is in constrast to the results of Refs. 14 and 86, in which no such separation from the crystal surface was observed.

Figure 28 shows the measured dependence of the cloud radius on excitation level. The radius in the x direction was obtained from the half-width at half maximum of the slit scans. It is clear from this data and from the profiles described above that the shape of the α cloud is neither spherical nor hemispherical, and that it does not scale in a simple way with P, at least in a crystal this small. How-

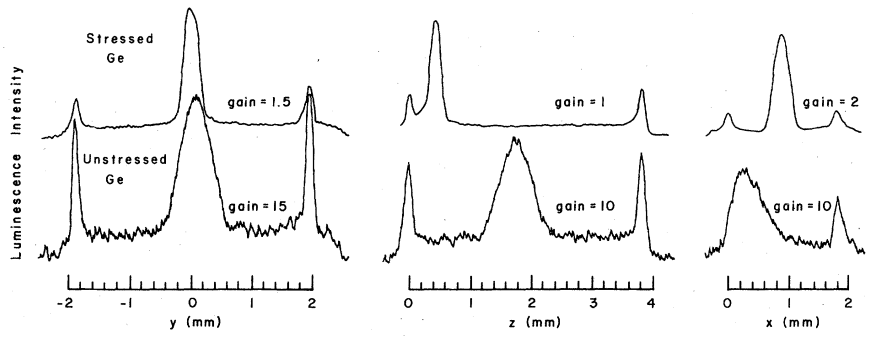

FIG. 24. Luminescence profiles for the same sample before and after the stress is removed. The upper row of scans is for a γ drop in the stressed sample, while the lower row of scans is for a cloud of α drops after the stress is removed. The crystal directions x, y, and z are defined in Sec. II. $P_{abs} = 2.8$ mW, $T = 1.8$ K.

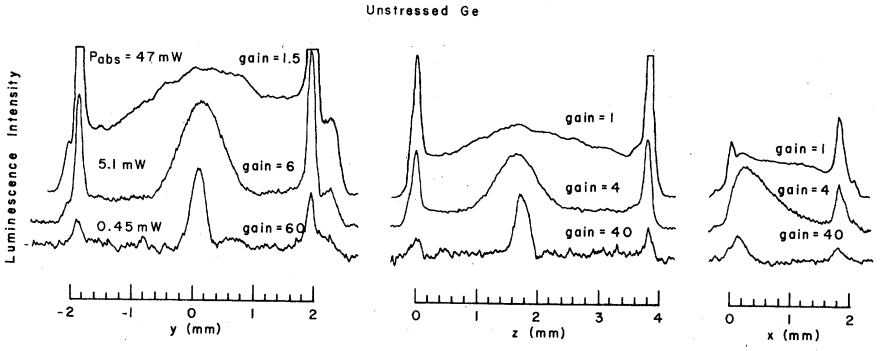

FIG. 25. Luminescence profiles for an unstressed sample. The upper row of scans is for $P_{abs}=47$ mW, the middle row is for $P_{abs}=5.1$ mW, and the lower row is for $P_{abs}=0.45$ mW. $T=1.8$ K.

ever, it is instructive to use a model of a hemispherical cloud to get an approximate value for the average e-h pair density within the cloud by comparison with the γ drop. Using just the α-cloud and γ-drop radii at equal P_{abs} (Fig. 24) and the measured $\tau_\alpha=36$ μsec and $\tau_\gamma=400$ μsec, we find from Eq. (14) that $n_{av}/\epsilon_{prod}\approx 1\times 10^{15}$ cm^{-3} for the cloud of α drops. This is consistent with the result of Voos *et al.*,[14] if ϵ_{prod} is close to ~100% for α drops.

In addition, the integrated luminescence intensity from a γ drop or a cloud of α drops (measured with the spectrometer slits removed) is proportional to $P_{abs}\times\epsilon_{prod}\times\epsilon_{rad}$. This quantity can also be estimated from the area under a slit scan. Using the areas under the curves in Fig. 24, we find $I_\gamma\approx 3.8 I_\alpha$, and hence

$$\epsilon_{rad\alpha}/\epsilon_{rad\gamma}\approx 0.3\,\epsilon_{prod\gamma}/\epsilon_{prod\alpha}\,. \tag{15}$$

Since the total intensities I_γ and I_α are both nearly proportional to P_{abs} over a wide range, Eq. (15) holds for a wide range of P. Since the production efficiency is likely to be smaller for γ drops than for α drops (due to the added difficulty of getting into the well), Eq. (15) shows that the radiative efficiency of α drops cannot be greater than about 30%,[91] somewhat lower than previous estimates.[44(b),72-74,78]

C. Time decays of the luminescence profiles

We have also observed the size of γ drops and α clouds as a function of time after the laser light is turned off. In the experiments, the laser light is square-wave modulated at 225 Hz, and the luminescence is sampled with a boxcar integrator at discrete times t after laser cutoff. Typical luminescence x scans are shown for γ drops in Fig. 29 ($t=0$ and $t=1000$ μsec) and for α clouds in Fig. 30 ($t=0$ and $t=100$ μsec), while Fig. 31 shows the radius versus delay time for x, y, and z scans for both cases. It is clear that the time behavior of γ drops and α clouds is quite different.

In Figs. 29 and 31(a) the γ-drop radii are mea-

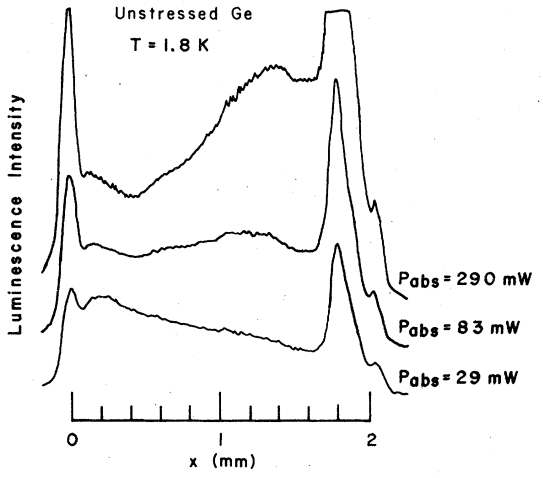

FIG. 26. Luminescence x scans for an unstressed sample at three moderate to high excitation levels. The laser is incident on the crystal face at $x=0$. The extra small peak at $x\approx 2$ mm is due to light scattered from the edge of the mirror. See Fig. 1(b) for the setup. $T=1.8$ K.

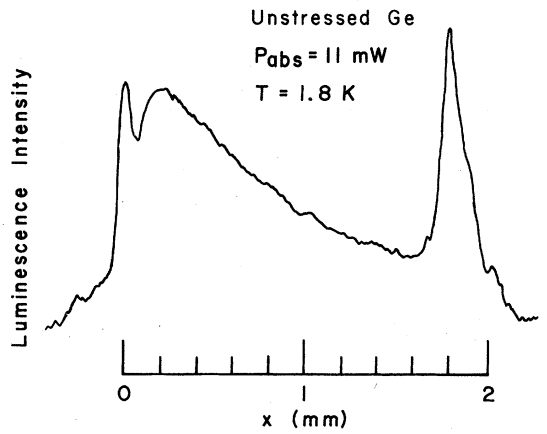

FIG. 27. Luminescence x scan for an unstressed sample at moderate excitation, $P_{abs}=11$ mW, showing the peak of the cloud to be separated from the face at $x=0$, where the laser is incident on the crystal. Resolution is ≈ 35 μm. $T=1.8$ K.

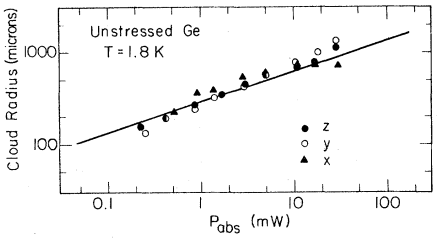

FIG. 28. Radius of the α cloud in unstressed Ge vs absorbed laser power P_{abs}. The solid line has a slope of $\frac{1}{3}$. $T = 1.8$ K.

sured at a relatively high light level $P_{abs} = 100$ mW. The decay is precisely what would be expected for the quasiequilibrium decay of a single drop: as the drop shrinks, its shape approximately corresponds to the steady-state shape of successively smaller drops (Fig. 22). The radius decay is nonexponential, analogous to the decay of the total luminescence at high excitation [see Fig. 16(b)].

Figure 32 shows the decay of the γ-drop radius for a sample stressed along $\langle 110 \rangle$, with $P_{abs} = 96$ mW. This sample was stressed in the "permanent-stress" geometry described in Ref. 4, so that both luminescence imaging and Alfvén resonance experiments could be done, using different experimental setups, for the same strain conditions. Shown also in an average radius inferred from Alfvén wave resonance.[11,16,20,92] The resonant absorption occurs at a magnetic field ($\vec{H} \| \langle 100 \rangle$) which varies with the drop size: $H \propto R$; and so the resonance shifts to lower fields as the drop decays. The Alfvén resonances were detected in a pulsed excitation experiment with 0.75 μJ/pulse, resulting in a smaller initial drop size. The resonance decay times measured in these two experiments are in good agreement. As expected (if compressional effects are not large), the radius decay time is approximately equal to three times the luminescence decay time.

On the other hand, the cloud of α drops in unstressed Ge decays in a quite different manner, as shown in Figs. 30 and 31(b). The size of the cloud

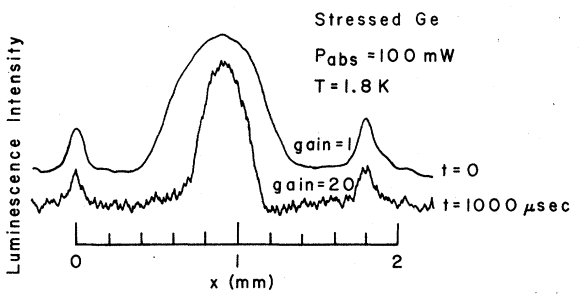

FIG. 29. Luminescence profiles for $t = 0$ and 1000 μsec for a sample stressed along $\langle 111 \rangle$. $P_{abs} = 100$ mW, $T = 1.8$ K.

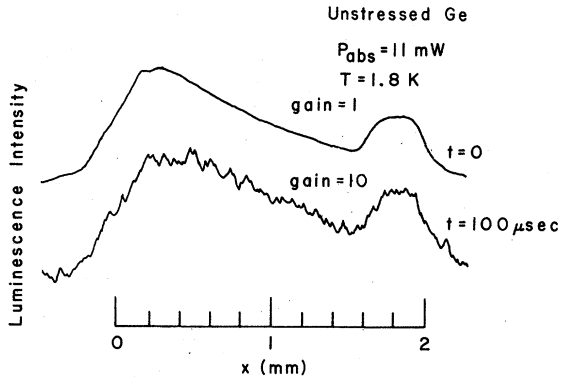

FIG. 30. Luminescence profiles for $t = 0$ and 100 μsec for an unstressed sample. $P_{abs} = 11$ mW, $T = 1.8$ K. Due to decreased spatial resolution (~330 μm) the edge effects at $x = 1.8$ mm are particularly broad.

does *not* decay in time at low temperature, implying that after the initial cloud formation the droplets individually decay at a relatively fixed position in the cloud. In Fig. 30, after 100-μsec delay the width of the luminescence profile is unchanged, even though the peak intensity has decreased by

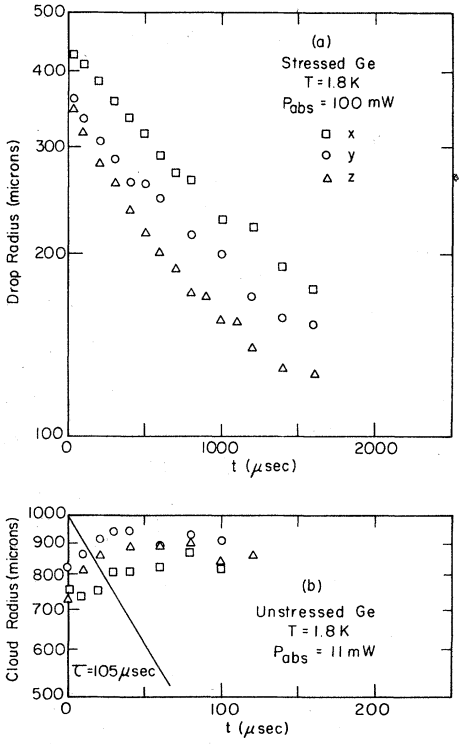

FIG. 31. Radii obtained from luminescence profiles. (a) γ-drop radii, for the same sample and conditions as in Fig. 29. (b) α-cloud radii, for the same conditions as in Fig. 30. The solid line assumes exponential decay at $\frac{1}{3}$ of the total luminescence decay, Fig. 16(c).

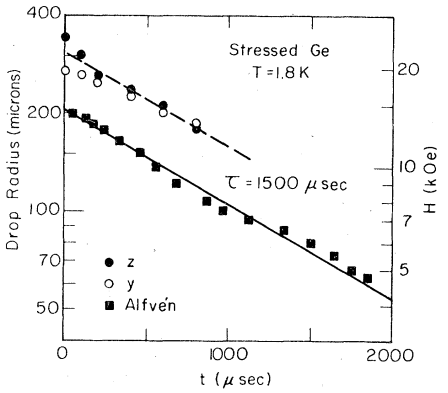

FIG. 32. Radius as a function of time for a sample stressed along ⟨110⟩, in the "permanent-stress" geometry of Ref. 4. (This stress direction would usually result in two strain wells. However, in this experiment the stress plunger was applied close to one edge of the sample, so that only a single minimum actually occurred inside the crystal.) ●, ○ from luminescence profiles, for $P_{abs}=96$ mW. ■ from Alfvén resonances, in a pulsed excitation experiment with 0.75 μJ/pulse, giving a smaller initial drop size; the radius is obtained from the resonant field as in Refs. 20 and 97, using $n=0.5\times10^{17}$ cm^{-3}. $T=1.8$ K.

over a factor of 10. In Fig. 31(b), the line corresponds to exponential decay with $\tau=105$ μsec. This is three times the luminescence decay time, which would be the expected radius decay time if the cloud decayed as a single body with $n_{av}=$ const. Clearly the cloud does not shrink in time: in fact, the data indicate the interesting possibility that the cloud size may initially *grow* after the light is switched off.

VI. DISCUSSION

We have shown that it is possible to produce large single drops of EHL in suitably strained Ge. When the drop is small enough, the e-h pair density is essentially uniform and the properties are characteristic of the liquid under uniform ⟨111⟩ uniaxial stress. The pair density is $n_\gamma=(0.50\pm0.05)\times10^{17}$ cm^{-3} ($T=1.6$–2.0 K, $-\sigma=4$–7 kgf/mm^2), as discussed in Secs. III D and III E. This is in comparison to the density for α drops, $n_\alpha=2.22\times10^{17}$ cm^{-3} (1.8 K).[2]

Vashishta, *et al.*, have estimated theoretically[9] that, for a ⟨111⟩ strain just large enough to depopulate three of the four conduction-band valleys [Ge(1:2) in the notation of Ref. 4], the pair density would be $n=0.69\times10^{17}$ cm^{-3} at $T=0$ (or $n=0.65\times10^{17}$ cm^{-3} at $T=1.8$ K).[80] However, they neglected the change of hole mass with stress. In Ref. 5 an attempt was made to estimate how significant this mass change was. Using three different models for the correlation energy, values of n ranging from (0.46 to 0.59)$\times10^{17}$ cm^{-3} were obtained ($T=0$ K, $\sigma_M=-6.5$ kgf/mm^2). Model 1, using the Vashishta *et al.* zero-stress correlation energy,[9] and assuming that the sum of exchange plus correlation energies is independent of stress, gives reasonable agreement with our experimental result, even when a T-dependent correction to n is included. Furthermore, this same model agrees with the densities derived from the uniform ⟨111⟩ stress data of Feldman *et al.*[29] and Pokrovskii *et al.*[30] over a range of stresses $-\sigma=5$–13 kgf/mm^2. Thus we conclude that the experimental determinations of the e-h pair density in the strain-confined EHL are in good agreement with the theoretical predictions.

A. Conduction-valley degeneracy in the strain-confined liquid

Theoretically, it is clear that a large ⟨111⟩ stress should split the four conduction-band valleys by a large enough amount that only a single band is occupied. This gives a clear explanation of the break in the slope of EHD peak luminescence versus stress, observed by Alekseev *et al.*[33] and Benoît à la Guillaume *et al.*[27] Similarly, it explains the sudden jumps we have observed in E_0, ΔE, τ, and I as functions of applied stress (Figs. 7 and 8). That is, the point of maximum shear stress in the sample does not become an energy minimum for the EHL until after the conduction-valley degeneracy is removed. However, it is of interest to consider what direct experimental evidence there is that only one conduction valley is occupied in γ drops.

The most direct evidence is given by the angle dependence of the ultrasonic attenuation, reported by Hansen.[93] The data were taken in a (110) plane over a range within 20° of the ⟨100⟩ direction, and show only a single series of magneto-oscillations. The angle dependence of the oscillation peaks is consistent with the variation of cyclotron mass[94] in the occupied valley. If all four valleys were occupied, there would be two other sets of peaks, corresponding to the cyclotron masses of the other valleys.

The conduction-valley degeneracy ν can be inferred indirectly by comparing our data on the luminescence linewidth (Sec. III D) and the magneto-oscillations of the luminescence (Sec. III E). The first measures the sum of the electron and hole Fermi energies $E_F^e+E_F^h$, while the second measures only the electron Fermi energy E_F^e. Specifically, we found $E_F=E_F^e+E_F^h\approx4.66$ meV from the luminescence linewidth, and $E_F^e\approx2.30$ meV from the magneto-oscillations. This yields

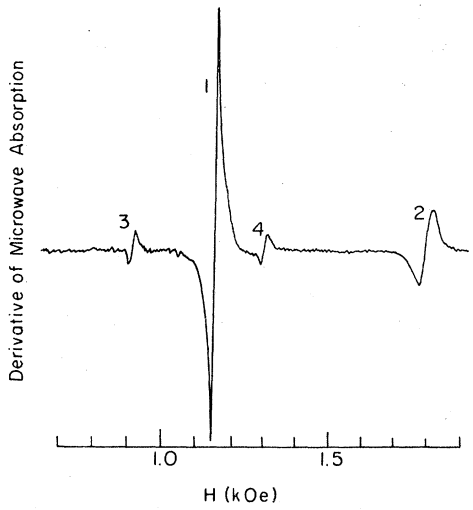

FIG. 33. Cyclotron resonance of carriers outside the γ drop in the same sample and strain configuration as in Fig. 32. The magnetic field was nearly parallel to a $\langle 100 \rangle$ crystal direction, but sufficiently off axis that the cyclotron resonance from electrons in each valley was separately resolved.

$E_F^h \approx 2.36$ meV which, for $T = 2.0$ K and $\sigma_M = -6.8$ kgf/mm^2, corresponds to $n \approx 0.47 \times 10^{17}$ cm^{-3}. This density in turn corresponds to $E_F^e = 2.15$ meV (for $\nu = 1$), 1.35 meV (for $\nu = 2$), or 0.85 meV (for $\nu = 4$). (These calculations all contain the assumption that the masses are unchanged from bulk Ge.[49]) Assuming that E_F^h may be approximately described by a scalar hole mass m_{dh}, this argument can be restated more quantitatively. Let $\gamma = m_{de}/m_{dh}$. Then

$$E_F = E_F^e (1 + \gamma \nu^{2/3}) . \tag{16}$$

Using the values $E_F = 4.66$ meV (luminescence linewidth), $E_F^e = 2.30$ meV (magneto-oscillations), $m_{de} = 0.22 m_0$, and $m_{dh} = 0.201 m_0$ [the *average* hole density-of-states mass for the line-shape calculation of Fig. 13(b)], Eq. (16) gives $\nu = 0.91$.[95] Thus the values we measure for E_F and E_F^e are consistent only if $\nu = 1$.

This degeneracy $\nu = 1$ can also be inferred from the angle dependence of the Alfvén resonances. The experimental result is quite striking. The resonance approximately follows the angle dependence of the electron-cyclotron resonance in a single ellipsoid, having 180° symmetry in a (110) plane characteristic of $\nu = 1$, rather than the 90° symmetry which would occur if $\nu = 4$. This angle dependence is expected theoretically.[92] The experiment was done on a crystal with a $\langle 1\bar{1}0 \rangle$ stress and a (110) face, the field being rotated in the plane of the crystal face. This geometry produces two drops, each having a different $\langle 111 \rangle$ ellipsoid occupied [Ref. 4, Fig. 29(c)]. The Alfvén resonances from the two drops could be observed separately, and, as expected, the peak in the angle dependence was separated by ~70° in the two drops.

Finally, Fig. 33 shows the cyclotron resonance of electrons outside the drop. The four peaks correspond to the four conduction-band valleys, and the different relative intensities indicate the relative populations of the valleys in the entire crystal. It is likely that most of the carriers are localized near the strain well. However, since the strain potential well acts as a repulsive barrier to electrons associated with other $\langle 111 \rangle$ valleys, it is likely that carriers not lowered in energy by the well will be located in other parts of the crystal. By varying the angle of the magnetic field it was confirmed that the electron valley associated with the largest cyclotron-resonance peak corresponds to the same $\langle 111 \rangle$ direction as that associated with the γ drop. Clearly, most of the carriers are located in a single valley, especially in the region of the potential well.

B. Advantages of large volumes of EHL for study

In similar stressed crystals, light scattering experiments[59-61] clearly showed that the γ drop is a continuous mass of fluid, and not a cloud of smaller drops. The large-angle scattering typical of Rayleigh-Gans scattering by small drops[3] vanished, leaving only an intense absorption near $\theta = 0$.

Having such a large mass of fluid allows the possibility of performing numerous experiments which would be impossible with a cloud of small drops. The Alfvén resonances[11,16,18,20,53,92] are direct probes of the drop size, which occur when the drop diameter is matched to a multiple of the microwave wavelength (inside the drop, where the wavelength is much shorter due to the high dielectric constant). Such resonances are not expected for the much smaller α drops in unstrained Ge,[11,96] except at much higher frequencies. These were the first experiments to actually probe the interior of the liquid, giving an estimate of carrier collision times. Using Alfvén resonances, it is possible to study the γ-drop buildup[97]: in a pulsed excitation experiment, the drop grows from zero to $R \approx 100$ μm in ≈ 1 μsec, requiring resolution on a time scale usually not accessible with the detectors used for studying luminescence.

Because the γ drop is formed in a strain well, it is possible to compress the EHL at a given temperature simply by increasing the size of the γ drop. This is in contrast to the case in unstressed Ge, where the density can be changed only by changing the temperature. Indeed, the compression of the γ drop shows up in all our data: the

luminescence linewidth, lifetime, period of magneto-oscillations of luminescence and ultrasonic attenuation, and power dependence of drop size. It can be explained quite straightforwardly by assuming that the chemical potential is constant across the γ drop.[5] We are presently making an extensive study of this phenomenon, to test the theory of the compressibility in detail.[32]

The internal particle dynamics, involving recombination currents and carrier-carrier collision times in the liquid, can be measured for the strain-confined liquid. A particularly striking effect is the distortion of the γ drop in an external magnetic field.[55-58] A hydrodynamic theory for the effect has been derived[98] which explains the general features and magnitude of the distortion. The observation and explanation of this phenomenon relies upon the ability to produce an image of a single large electron-hole drop.

Finally, the strain-confined liquid is useful in determining the energetics of the Fermi liquid under stress. For sufficiently small radius ($R \lesssim 150$ μm) the liquid occupies a region of relatively uniform strain, and the measured pair density is in good agreement with theoretical predictions for uniaxially stressed Ge, i.e., for Ge (1:2). The strain gradient however provides a useful inhibiting effect on the liquid evaporation, permitting a measurement of the volume decay time under stress. Given a refined theory, a knowledge of the strain dependence of τ promises to reveal detailed information about the various recombination processes in the EHL.

ACKNOWLEDGMENTS

We thank E. E. Haller and W. L. Hansen for providing the ultrapure Ge crystals and many useful suggestions. C. Kittel provided helpful ideas through the course of these experiments. One of us (J.P.W.) was supported in part during the writing of this paper by NSF Grant DMR-76-01058. One of us (R.S.M.) was supported by an IBM fellowship when most of the experimental work was complete. One of us (J.E.F.) was supported by an NSF fellowship when most of the experimental work was completed. This work was supported in part by the Division of Basic Energy Sciences, U.S. Department of Energy.

---

*Present address: Physics Dept. and Materials Research Laboratory, University of Illinois, Urbana, Ill. 61801.

†Present address: Physical Science Branch, General Electric Co., Corporate Research and Development, Schenectady, N. Y. 12345.

[1]L. V. Keldysh, in *Proceedings of the Ninth International Conference on the Physics of Semiconductors, Moscow* (Nauka, Leningrad, 1968), p. 1303; L. V. Keldysh, *Eksitonyv Poluprovodnikakh (Excitons in Semiconductors* (Izd. Nauka, Moscow, 1971), p. 5.

[2]For reviews see (a) Ya. Pokrovskii, Phys. Status Solidi B 11, 385 (1972); (b) C. D. Jeffries, Science 189, 955 (1975); (c) J. C. Hensel, T. G. Phillips, and G. A. Thomas, *Solid State Physics*, edited by H. Enrenreich, F. Seitz, and D. Turnbull (Academic, New York, Vol. 32, p. 88; (d) T. M. Rice, *ibid.*, p. 1.

[3]Ya. E. Pokrovskii and K. I. Svistunova, Zh. Eksp. Teor. Fiz. Pis'ma Red. 13, 297 (1971) [JETP Lett. 13, 212 (1971)]; J. M. Worlock, T. C. Damen, K. L. Shaklee, and J. P. Gordon, Phys. Rev. Lett. 33, 771 (1974).

[4]R. S. Markiewicz, J. P. Wolfe, and C. D. Jeffries, Phys. Rev. B 15, 1988 (1977).

[5]R. S. Markiewicz and S. M. Kelso, Solid State Commun. 25, 275 (1978).

[6]W. F. Brinkman and T. M. Rice, Phys. Rev. B 7, 1508 (1973).

[7]M. Combescot and P. Nozières, J. Phys. C 5, 2369 (1972).

[8]P. Bhattacharyya, V. Massida, K. S. Singwi, and P. Vashishta, Phys. Rev. B 10, 5127 (1974).

[9]P. Vashishta, R K. Kalia, and K. S. Singwi, in *Lecture Notes in Physics*, edited by M. Ueta and Y. Nishina (Springer-Verlag, Heidelberg, 1976), Vol. 57, p. 187; P. Vashishta (private communication).

[10]P. Vashishta, P. Bhattacharyya, and K. S. Singwi, Phys. Rev. B 10, 5108 (1974).

[11]R. S. Markiewicz, thesis (University of California, 1975) (unpublished).

[12]J. P. Wolfe, R. S. Markiewicz, and C. D. Jeffries, in *Proceedings of the Third International Conference on Light Scattering in Solids, Campinas*, edited by R. C. C. Leite (Flammarion, Paris, 1975), p. 173; C. D. Jeffries, J. P. Wolfe, and R. S. Markiewicz, in *Proceedings of the Thirteenth International Conference on the Physics of Semiconductors, Rome*, edited by F. G. Fumi (Tipografia Marves, Rome, 1976), p. 879.

[13]H. Hertz, J. Rein. Ang. Math. 92, 156 (1881).

[14]M. Voos, K. L. Shaklee, and J. M. Worlock, Phys. Rev. Lett. 33, 1161 (1974).

[15]R. W. Martin, thesis (Stuttgart, 1974) (unpublished); R. W. Martin, Phys. Status Solidi B 61, 223 (1974).

[16]J. P. Wolfe, R. S. Markiewicz, C. Kittel, and C. D. Jeffries, Phys. Rev. Lett. 34, 275 (1975).

[17]W. L. Hansen and E. E. Haller, IEEE Trans. Nucl. Sci. 21, 251 (1974).

[18]C. D. Jeffries, J. P. Wolfe, S. M. Kelso, R. S. Markiewicz, and J. E. Furneaux, J. Lumin. 12, 659 (1976).

[19]This is calculated from the optical coefficients of Ge, $n = 5.06$ and $k = 2.50$ at 5145 Å and 120 K. [R. F. Potter, Phys. Rev. 150, 562 (1966).] The coefficients are not expected to change appreciably below that temperature. [Y.-R. Shen (private communication).]

[20]R. S. Markiewicz, J. P. Wolfe, and C. D. Jeffries, Phys. Rev. Lett. 32, 1357 (1974); 34, 59(E) (1975).

[21]See, for example, R. M. Westervelt, *Proceedings of*

the Thirteenth International Conference on the Physics of Semiconductors, Rome, edited by F. G. Fumi (Tipografia Marves, Rome, 1976), p. 902; J. C. Hensel, T. G. Phillips, and T. M. Rice, Phys. Rev. Lett. 30, 227 (1973); T. K. Lo, B. J. Feldman, and C. D. Jeffries, Phys. Rev. Lett. 31, 224 (1973).

[22]The change in ϕ with stress can be estimated from experimental results on the shift of EHL and exciton luminescence with stress: compare Fig. 6 of Ref. 27 with Fig. 10 of Ref. 38; see also, T. Ohyama, T. Sanada, and E. Otsuka, Phys. Rev. Lett. 33, 647 (1974).

[23]J. E. Furneaux, R. S. Markiewicz, and S. M. Kelso, Bull. Am. Phys. Soc. 22, 270 (1977).

[24]J. E. Furneaux, R. S. Markiewicz, S. M. Kelso, and C. D. Jeffries (unpublished).

[25]G. A. Thomas, A. Frova, J. C. Hensel, R. E. Miller, and P. A. Lee, Phys. Rev. B 13, 1692 (1976).

[26]R. M. Westervelt, in Ref. 21; R. M. Westervelt, thesis (University of California, 1977) (unpublished); R. M. Westervelt (unpublished).

[27]C. Benoît à la Guillaume, M. Voos, and F. Salvan, Phys. Rev. B 5, 3079 (1972).

[28]In principle, the strains could be calibrated by observing the strain-induced birefringence pattern (see Ref. 4). In practice, this is difficult, since the birefringence represents a two-dimensional average of the three-dimensional strain pattern. Furthermore, great care must be taken to avoid interference effects. If the crystal surfaces are not optically smooth, or if the polarized beam is not everywhere perpendicular to the surface, there will be interference between different rays of light, which tends to blur the pattern, reducing the number of fringes. Thus, while the fringes shown in Ref. 4 correctly reflect the distribution of strain in the crystal, they probably underestimate the magnitudes of the strains by about a factor of 2.

[29]B. J. Feldman, H.-h. Chou, and G. K. Wong, Bull. Am. Phys. Soc. 22, 269 (1977), and unpublished results.

[30]Ya. E. Pokrovskii and K. I. Svistunova, Zh. Eksp. Teor. Fiz. 68, 2323 (1975) [Soviet Phys.-JETP 41, 1161 (1976)].

[31]S. M. Kelso, R. S. Markiewicz, and J. E. Furneaux, Bull. Am. Phys. Soc. 22, 269 (1977).

[32]S. M. Kelso, R. S. Markiewicz, J. E. Furneaux, and C. D. Jeffries (unpublished).

[33]See, for example, A. S. Alekseev, V. S. Bagaev, and T. I. Galkina, Zh. Eksp. Teor. Fiz. 63, 1020 (1972). [Sov. Phys.-JETP 36, 536 (1973)]; T. Ohyama, T. Sanada, K. Fujii, and E. Otsuka, in *Proceedings of the Twelfth International Conference on the Physics of Semicondutors, Stuttgart*, edited by M. H. Pilkuhn (Teubner, Stuttgart, 1974), p. 66; and Ref. 27. The greatly decreased lifetime and luminescence intensity observed in these experiments may have been due to nonuniformity in the stress, driving the drops into rapid recombination centers at the crystal surface. Also, we have observed shorter lifetimes for γ drops when dislocated samples were used. Pokrovskii (Ref. 60) has recently reported lifetimes of ≈ 400 μsec in dislocation-free Ge under uniaxial $\langle 111 \rangle$ stress, where the lifetime did not vary greatly with stress.

[34]Note that, for the sample stressed along $\langle 100 \rangle$, the luminescence is scarcely shifted from its unstressed position—indeed the peak is actually shifted to higher energy than in the unstressed sample. This does not mean that drops are not attracted to the well. A *uniaxial* $\langle 100 \rangle$ stress raises the EHL pair energy (Ref. 27), but in the inhomogeneously stressed sample, the pair energy is raised everywhere except in the wells, as shown in Fig. 10 of Ref. 4. Actually, the γ-drop luminescence line in Fig. 9 is sufficiently narrow that the high-energy edge is at a lower energy than in the unstressed sample, showing that the γ drop is in a lower-energy state.

[35]The density is also expected to vary with position in the well, due to the change in stress. However, the theory of Ref. 5 and the data of Ref. 29 indicate that n varies only weakly with uniform stress over the range relevant to this discussion ($-\sigma = 4$–6 kgf/mm^2 for a 400-μm radius drop).

[36]Ya. Pokrovskii, A. Kaminskii, and K. Svistunova, in *Proceedings of the Tenth International Conference on the Physics of Semiconductors, Cambridge*, edited by S. P. Keller, J. C. Hensel, and F. Stern (U.S. E.A.C. 1970), p. 504.

[37]C. Benoît à la Guillaume and M. Voos, Phys. Rev. B 7, 1723 (1973).

[38]I. Balslev, Phys. Rev. 143, 636 (1966).

[39]K. Suzuki and J. C. Hensel, Phys. Rev. B 9, 4184 (1974); J. C. Hensel and K. Suzuki, Phys. Rev. B 9, 4219 (1974).

[40]M. E. Fine, J. Appl. Phys. 26, 862 (1955).

[41]At low P, the lines we observe are slightly narrower than those seen in Ref. 29. This may be because of inhomogeneous broadening due to small inhomogeneities in the "uniform" stress experiment. This is a problem of considerable difficulty attending all experiments of uniform stress on EHD (see Ref. 33).

[42]H. L. Störmer, R. W. Martin, and J. C. Hensel, in *Proceedings of the Thirteenth International Conference on the Physics of Semiconductors, Rome*, edited by F. G. Fumi (Tipografia Marves, Rome, 1976), p. 950; R. W. Martin and H. L. Störmer, Solid State Commun. 22, 523 (1977).

[43]G. A. Thomas and M. Capizzi, in *Proceedings of the Thirteenth International Conference on the Physics of Semiconductors, Rome*, edited by F. G. Fumi (Tipografia Marves, Rome, 1976), p. 914.

[44](a) V. S. Bagaev, T.I. Galkina, N. A. Penin, V. B. Stopachinskii, and M. N. Churaeva, Zh. Eksp. Teor. Fiz. Pis'ma Red. 16, 120 (1972) [JETP Lett. 16, 83 (1972)]; (b) K. Betzler, B. G. Zhurkin, and A. L. Karuzskii, Solid State Commun. 17, 577 (1975); and K. Betzler, B. G. Zhurkin, A. L. Karuzskii, and B. M. Balter, J. Lumin. 12, 651 (1976).

[45]V. N. Murzin, V. A. Zayats, and V. L. Kononenko, Fiz. Tverd. Tela 15, 3634 (1973) [Sov. Phys.-Solid State 15, 2421 (1974)].

[46]K. Fujii and E. Otsuka, J. Phys. Soc. Jpn. 38, 742 (1975).

[47]Oscillations in the photocurrent initially ascribed to holes in EHD, in V. F. Gantmakher and V. N. Zverev, Zh. Eksp. Teor. Fiz. Pis'ma Red. 18, 180 (1973) [JETP Lett. 18, 105 (1973)], have been reinterpreted. See. V. F. Gantmakher and V. N. Zverev, Zh. Eksp. Teor. Fiz. 69, 695 (1975). [Sov. Phys.-JETP 42, 352 (1975)].

[48]The luminescence intensity usually had an overall monotonic decrease with field, in addition to the

oscillations. This may have been due in part to reduced pumping efficiency of carriers into the strain well.

[49]Rice has calculated renormalized carrier masses in EHD in unstressed Ge, and finds for electrons $m_{\parallel}$(EHD) $\approx 0.99 m_{\parallel}$(Ge), $m_{\perp}$(EHD) $\approx 1.10 m_{\perp}$(Ge); for holes m_{lh}(EHD) $\approx 1.10 m_{lh}$(Ge), m_{hh}(EHD) $\approx 1.14 m_{hh}$(Ge). See T. M. Rice, Nuovo Cimento B 23, 226 (1974).

[50]L. V. Keldysh and A. P. Silin, Fiz. Tverd. Tela 15, 1532 (1973) [Sov. Phys.-Solid State 15, 1027 (1973)].

[51]T. Ohyama, A. D. A. Hansen, and J. L. Turney, Solid State Commun. 19, 1083 (1976); A. D. A. Hansen, T. Ohyama, and J. L. Turney, Lecture Notes of Third International Conference on the Application of High Magnetic Fields in Semiconductor Physics, Würzburg (Physikalisches Institut der Universitat Würzburg, 1976) (unpublished), p. 580.

[52]A. D. A. Hansen (private communication).

[53]R. S. Markiewicz, Phys. Rev. B 10, 1766 (1974).

[54]Reference 18 quoted a value $n_{\gamma} = 0.7 \times 10^{17}$ cm^{-3}, while Ref. 11 quoted a value $n_{\gamma} = 1 \times 10^{17}$ cm^{-3}. This difference is due to an overall decrease in drop *volume* in a magnetic field, which was taken into account only in Ref. 11. However, experiments subsequent to those in Refs. 11 and 18, involving simultaneous imaging and Alfvén absorption measurements, showed the distortion of the drop *shape* in a magnetic field. Assuming the primary resonance observed is the longitudinal magnetic dipole resonance, the field configurations indicate that the drop dimension perpendicular to the external field would be measured (see Ref. 11, especially Fig. IV.1a–1b). Since this is generally the larger dimension, the lower value for n is more nearly correct.

[55]R. S. Markiewicz, J. E. Furneaux, and J. P. Wolfe, Bull. Am. Phys. Soc. 21, 223 (1976); J. P. Wolfe, J. E. Furneaux, and R. S. Markiewicz, *Proceedings of the Thirteenth International Conference on the Physics of Semiconductors, Rome*, edited by F. G. Fumi (Tipografia Marves, Rome, 1976), p. 954.

[56]H. L. Störmer and D. Bimberg, Comments Phys. 1 (5), 131 (1976).

[57]D. Bimberg and H. L. Störmer, Nuovo Cimento B 39, 615 (1977).

[58]J. P. Wolfe, R. S. Markiewicz, J. E. Furneaux, S. M. Kelso, and C. D. Jeffries, Phys. Status Solidi B 83, 305 (1977).

[59]Ya. E. Pokrovskii and K. I. Svistunova, Zh. Eksp. Teor. Fiz. Pis'ma Red. 23, 110 (1976). [JETP Lett. 23, 95 (1976)].

[60]Ya. E. Pokrovskii and K. I. Svistunova, *Proceedings of the Thirteenth International Conference on the Physics of Semiconductors, Rome*, edited by F. G. Fumi (Tipografia Marves, Rome, 1976), p. 849.

[61]J. C. V. Mattos, J. M. Worlock, and T. C. Damen, Solid State Commun. 22, 13 (1977).

[62]For a recent measurement of σ_a, see M. Glicksman, S. A. Mittleman, P. Joshi, and J. R. Meyer, Bull. Am. Phys. Soc. 22, 350 (1977). There is a misprint in the abstract, and σ_a(3.39 μm) $\simeq 4.5 \times 10^{-17}$ cm^2 [M. Glicksman (private communication)]. Pokrovskii and Svistunova, in Ref. 60, used $\sigma_a = 1.5 \times 10^{-16}$ cm^2; Mattos *et al.*, in Ref. 61, used $\sigma_a = 3 \times 10^{-17}$ cm^2.

[63]R. L. Aurbach, L. Eaves, R. S. Markiewicz, and P. L. Richards, Solid State Commun. 19, 1023 (1976).

[64]M. Combescot and P. Nozières, Solid State Commun. 10, 301 (1972).

[65]V. N. Murzin, Fiz. Tekh. Poluprovodn. 7, 1610 (1973) [Sov. Phys. Semiconductors 7, 1074 (1974)].

[66]T. M. Rice, Bull. Am. Phys. Soc. 20, 470 (1975); J. H. Rose and H. B. Shore, *ibid.*, 20, 470 (1975).

[67]J. H. Rose, H. B. Shore, and T. M. Rice, Phys. Rev. B 17, 752 (1978).

[68]V. N. Murzin, V. A. Zayats, and V. L. Kononenko, Fiz. Tverd. Tela 17, 2684 (1975) [Sov. Phys. Solid State 17, 1783 (1976)].

[69]A similar calculation for γ drops in complicated by the inhomogeneous strain, but this strain also weakens the intensity of interband transitions. A. Manoliu (private communication, 1975).

[70]A. S. Alekseev, V. S. Bagaev, T. I. Galkina, O. V. Gogolin, and N. A. Penin, Fiz. Tverd. Tela 12, 3516 (1970) [Sov. Phys. Solid State 12, 2855 (1971)]; C. Benoît à la Guillaume and M. Voos, Solid State Commun. 11, 1585 (1972); R. W. Martin and R. Sauer, Phys. Status Solidi B 62, 443 (1974).

[71]Ya. E. Pokrovskii (private communication); R. M. Westervelt (private communication).

[72]Ya. E. Pokrovskii and K. I. Svistunova, Fiz. Tekh. Poluprovodn. 4, 491 (1970) [Sov. Phys. Semicond. 4, 409 (1970)].

[73]C. Benoît à la Guillaume, M. Voos, and F. Salvan, Phys. Rev. Lett. 27, 1214 (1971).

[74]R. F. Leheny, J. Shah, and M. Voos, Solid State Commun. 20, 819 (1976).

[75]R. M. Westervelt, T. K. Lo, J. L. Staehli, and C. D. Jeffries, Phys. Rev. Lett. 32, 1051 (1974); 32, 1331(*E*) (1974).

[76]C. Benoît à la Guillaume, M. Capizzi, B. Etienne, and M. Voos, Solid State Commun. 15, 1031 (1974).

[77]J. C. Hensel, T. G. Phillips, and T. M. Rice, Phys. Rev. Lett. 30, 227 (1973).

[78]Ya. E. Pokrovskii (private communication). This value is somewhat lower than published values (Refs. 44b, 72–74). However, the absolute measure of ϵ_{rad} is experimentally very difficult and is subject to error. Pokrovskii and Svistunova (Ref. 60) have found that the quantum efficiency is at least three times greater in their uniformly stressed samples than in unstressed Ge.

[79]P. Vashishta, S. G. Das, and K. S. Singwi, Phys. Rev. Lett. 33, 911 (1974).

[80]$n = 0.69 \times (1 - 0.0189\ T^2) \times 10^{17}$ cm^{-3} for Ge(1:2). P. Vashishta (private communication).

[81]T. K. Lo, Solid State Commun. 15, 1231 (1974).

[82]G. A. Thomas, T. G. Phillips, T. M. Rice, and J. C. Hensel, Phys. Rev. Lett. 31, 386 (1973).

[83]J. P. Wolfe, W. L. Hansen, E. E. Haller, R. S. Markiewicz, C. Kittel, and C. D. Jeffries, Phys. Rev. Lett. 34, 1292 (1975).

[84]P. Vashishta, R. K. Kalia, and K. S. Singwi, Solid State Commun. 19, 935 (1976).

[85]B. J. Feldman, Phys. Rev. Lett. 33, 359 (1974).

[86]J. C. V. Mattos, K. L. Shaklee, M. Voos, T. C. Dayem, and J. M. Worlock, Phys. Rev. B 13, 5603 (1976).

[87]V. S. Bagaev, L. V. Keldysh, N. N. Sibel'din, V. A. Tsvetkov, Zh. Eksp. Teor. Fiz. 70, 702 (1976) [Sov. Phys. JETP 43, 362 (1976)].

[88]J. Doehler, J. C. V. Mattos, and J. M. Worlock, Phys. Rev. Lett. 38, 726 (1977).

[89]J. C. Hensel and R. C. Dynes, Bull. Am. Phys. Soc. 22, 349 (1977); Phys. Rev. Lett. 39, 969 (1977).

[90]Other possible mechanisms for producing the "cloud" are possible. See M. Combescot, Phys. Rev. B 12, 1591 (1975); I. Balslev and J. M. Hvam, Phys. Status Solidi B 65, 531 (1974); J. M. Hvam and I. Balslev, Phys. Rev. B 11, 5053 (1975); and the discussion in Refs. 87 and 89.

[91]From the estimates given in the text, $\epsilon_{\text{prod}\gamma} \approx 30\%$ and $\epsilon_{\text{prod}\alpha} \approx 100\%$, Eq. (15) gives a value ≈ 0.1, which we consider to be a lower limit on the ratio of radiative efficiencies.

[92]R. S. Markiewicz (unpublished).

[93]A. D. A. Hansen and T. Ohyama, Bull. Am. Phys. Soc. 22, 269 (1977); and A. D. A. Hansen, thesis (University of California, Berkeley, 1977) (unpublished), especially Fig. 81.8.

[94]See, for example, C. Kittel, *Introduction to Solid State Physics*, 5th ed. (Wiley, New York, 1976), p. 227

[95]In general, there can be an unequal population of electrons in the various valleys corresponding to noninteger ν. Our result can be taken to indicate that the population of three of the four valleys is much less than the remaining valley.

[96]J. R. Dixon, Jr., and J. K. Furdyna, Phys. Rev. B 13, 3657 (1976).

[97]J. E. Furneaux, J. P. Wolfe, and C. D. Jeffries, Solid State Commun. 20, 317 (1976).

[98]R. S. Markiewicz, Phys. Rev. B 17, 4788 (1978); R. S. Markiewicz, H. Hurwitz, Jr., and R. S. Likes, Phys. Rev. B (to be published).

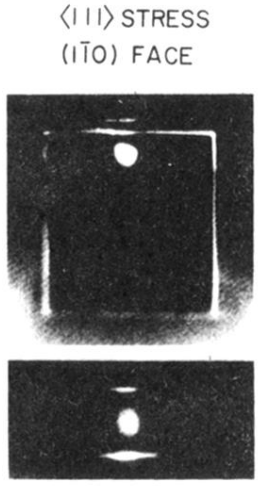

FIG. 20. Luminescence image from a sample stressed in the ⟨111⟩ direction, viewed through a (110) face and displayed using an infrared vidicon and standard TV monitor. Lower photo is an end view through a (111) face, as shown in Fig. 1(b). The crystal face pumped by the laser is uppermost in the end view. $P_{abs} = 90$ mW, $T = 1.8$ K.